RESEARCH PAPER

Unique Identification of Stiffness Parameters in Hyperelastic Models for Anisotropic, Deformable, Thin Materials Based on a Single Experiment - A Feasibility Study Based on Virtual Full-Field Data

L. Makhool[1] · D. Balzani[1]

© The Author(s) 2024

Abstract

Background Characterizing material properties of thin sheets for design or manufacturing purposes is an essential concern in many engineering applications. This task is particularly challenging for materials with a pronounced anisotropic and nonlinear mechanical behavior.

Objective A hybrid, experimental-numerical approach for the characterization of the mechanical, nonlinear response of thin, anisotropic, deformable materials is proposed. In contrast to classical approaches where various biaxial tension tests are analyzed, the main goal here is the complete characterization based on one single experiment.

Methods The proposed approach is based on a novel non-standard experimental setup which is on the one hand easy to install and use, and which on the other hand intentionally induces a strongly inhomogeneous strain field in the specimen capturing as many deformation modes and intensities as possible. The resulting displacement field can be measured using e.g., digital image correlation, and is then accessible to the parameter identification as full-field data. To allow for an efficient identification, an extended equilibrium gap method is presented, where unknown boundary force distributions applied in the experiment are computed iteratively. The approach's feasibility is assessed through virtual full-field data obtained by numerical simulation of the proposed experimental setup using predefined parameter values and applying realistic noise. That way, a quantitative assessment of the method's performance regarding two specifically chosen material models is enabled.

Results Provided that the stiffness-related material parameters are indeed linear in the stress equations, a quadratic optimization problem can be constructed to allow for a unique identification of the parameter values. Analysis show that reference parameter values for calendered rubber as well as coated textile fabric can be identified, even when realistic noise is applied to the virtual test data.

Conclusion Based on the presented investigations, the proposed method has been found to be feasible for the accurate identification of stiffness-related parameters of anisotropic, nonlinear thin sheets using a single experiment.

Keywords Inverse analysis · Unique identification of material parameters · Nonlinear anisotropic material response · Large strains

Introduction

Performing predictive and accurate simulations of structural engineering problems is important for a wide range of applications including e.g., the optimization of design tasks or manufacturing processes. In the case of nonlinear, anisotropic, thin materials such as e.g., calendered rubber, coated textile fabrics or biological membranes, appropriate constitutive models are required which specifically describe the mechanical behavior of the considered materials within their plane perpendicular to the thickness direction. In the context of nonlinear, anisotropic materials, a variety of models has been proposed in the literature and is also available in commercial finite element (FE) programs. However, aside from the models themselves, the included material parameters play an important role with view to having quantitatively meaningful predictions of the analyzed structural problems. Thus, a methodology enabling an efficient quantitative identification of the parameters' values is required. Furthermore, a unique identification becomes essential if also the

✉ D. Balzani
daniel.balzani@ruhr-uni-bochum.de

[1] Chair of Continuum Mechanics, Ruhr-Universität Bochum
Universitätsstraße 150, 44801 Bochum, Germany

values themselves are needed to carry information. This is for instance important in classical engineering tasks where values of parameters are to be tabulated for standardized usage. Conventionally, uniaxial/biaxial tension and shear tests performed on planar specimen sheets are widely used as a standard approach in material parameter identification since they are straightforward to employ, and the resultant homogeneous stress and strain fields are well understood. A single uniaxial tension test is sufficient to fully identify the parameters of isotropic, linear elasticity, namely the Young's modulus and the Poisson's ratio, if the lateral contraction is measured along with the axial strain. However, when nonlinearity and anisotropy are under investigation, single uniaxial tests alone do not produce sufficient data to characterize such materials. Therefore, a set of different tests, still providing homogeneous stress and strain fields, performed in different directions, is usually considered. Based on the collected stress-strain data, the material parameters can be identified by minimizing an least-square objective function formulated in terms of differences of the model response and the experimental data.

Substantial body of literature deals with the identification of parameters of hyperelastic, nearly incompressible materials based on experimental characterization. Starting with isotropic hyperelasticity, the researchers in [1] captured the nonlinear isotropic behavior of a rubber material by adjusting the Ogden model to experimental data obtained from three different tests: simple tension, equibiaxial tension, and pure shear [2]. Furthermore, an experimental setup has been developed in [3] to allow for the characterization of polymers based on varying biaxial loading. For nonlinear anisotropic materials, a uniaxial tension test applied in two directions [4] has been employed to characterize the anisotropic behavior of calendered rubber. The anisotropic form of an Ogden hyperelastic strain energy density function has been adjusted to biaxial tension test data performed on the brain white material [5]. Extensive research has been invested regarding composite materials of varying types. For instance, an anisotropic hyperelastic constitutive model for a cord/rubber composite has been developed in [6], accounting for the cord-rubber normal and shear interaction. The constitutive model has been fitted to a group of experimental data to identify the material parameters in the model. Uniaxial tension was applied on the individual components, pure rubber and pure reinforcements, in the transversal direction and on 22° off-axis to characterize the rubber, the cord, the normal and shear interaction, respectively. In the context of biological tissues, uniaxial tests performed in different directions are often considered as basis for parameter identification, cf. e.g., [7]. In order to also address the independent response of matrix and included fibers, the researchers in [8] adjusted a model for annulus fibrosus also based on multiple tests. For coated textile membranes, a set of 5 cyclic biaxial tension tests with varying load ratios is considered standard to characterize appropriate material models, see [9, 10], and several cycles are usually required to identify the saturated elastic response [11].

All these approaches, which are based on rather classical experiments, are characterized by a substantial effort required to obtain a suitable parameter adjustment. This results mainly from the fact that only homogeneous stress/strain fields are analyzed in the individual tests. This, in turn, requires the consideration of multiple tests to obtain data on varying loading scenarios. In fact, the more parameters are to be identified, the more tests are usually required. Thus, it appears promising to consider inhomogeneous, full-field kinematics to include multiple deformation modes into the parameter adjustment procedure already by a single test or at least very few tests. The current development of devices for the measurement of such kinematic fields facilitates the characterization of the material behavior by solving the *inverse problem*, where usually the material parameters are identified such that the full field kinematics obtained from a structural simulation of the test setup match best the experimental measurement. The structural simulation as important part therein, is usually referred to as the *forward problem*. Thereby, the inverse problem can be interpreted as a hybrid numerical-experimental approach which is mainly composed of three central units: the Finite Element (FE) model simulating the experiment, the experimental data in terms of full-field measurements, and finally, the optimization approach returning the optimal material parameters. Note that we refer to "full-field" data as soon as selected regions with inhomogeneous mechanical fields are taken into account as full fields. The data does not necessarily need to be available for the whole structure.

The advancement of experimental devices as well as computational technologies has promoted the development of various approaches for parameter adjustment based on full-field data. An overview of such strategies can be found in [12]. The Finite Element Model Updating (FEMU), first proposed in [13], minimizes the discrepancy between data resulting from a finite element model and their counterpart extracted from the experiment. The utilized data in the FEMU can be either forces (FEMU-F) [14], displacements (FEMU-U) [15], or a combination of both (FEMU-U-F) [16]. A discussion of benefits and disadvantages of each method can be found in [17]. The Constitutive Equation Gap Method (CEGM) [18] minimizes the distance between a given stress field and another one computed from measured displacements through a constitutive equation. The Virtual Field Method (VFM) [19] relies on the virtual work principle, where the strain field derived from the measured displacements as well as the loading conditions are regarded to be known. Therein, a parametric stress field is derived, where the stress components depend on the

unknown parameters at any point across the domain of interest. Then, a set of scalar equations of unknown parameters is obtained after applying the principle of virtual work. Generating virtual fields is an essential step in the VFM, and various approaches have been proposed for this purpose, see e.g., [12]. However, this step remains challenging, since different strategies can lead to different results. In [20], a feasibility study of the VFM has been carried out to identify the parameters of isotropic hyperelastic materials using the nonlinear models of Neo-Hookean, Mooney-Rivlin and Veronda-Westmann. The potential application of the proposed approach is biomedical engineering, i.e. the identification of the lamina cribosa. Furthermore, in [21], the identification of the heterogeneous distribution of hyperelastic parameters of soft tissues has been conducted on the basis of VFM. In the mentioned two works, the forward problem is solved iteratively until convergence is achieved. A variant of the VFM is the Reciprocity Gap Method (RGM) [22], where the applied traction and the full-field measurements are available only on the boundary of the domain. In the Equilibrium Gap Method (EGM), a measured kinematic field serves as direct input to a computational model and then, the material parameters are identified from minimizing the distance to satisfying the mechanical equilibrium equations. Derivation of EGM with increasing the complexity from identifying homogeneous elastic properties to heterogeneous properties has been documented in [23]. Furthermore, damage growth laws in orthotropic composite materials have been identified in [24].

Mainly, the strategies for solving inverse problems using full-field data can be categorized into two groups: updating methods (FEMU-U, FEMU-U-F, CEGM, and RGM) and non-updating methods (FEM-F, EGM, and VFM). For the first group, the solution of the forward problem is updated in each iteration of the optimization procedure. Especially in the context of nonlinear mechanical problems, each solution may be computationally expensive and time-consuming for relevant practical applications. Furthermore, in these types of strategies, the objective function depends on displacements which makes it dependent on geometrical and physical nonlinearities. Thus, a unique identification can generally not be obtained if materially nonlinear mechanical problems are considered since the objective function is no longer convex. These drawbacks can be overcome in the non-updating approaches by inserting the measured displacements into the FE model, which is then purely evaluated considering the constitutive parameters and hence computationally cheap. Most important, however, is that the physical and/or geometrical nonlinearity in the forward problem does not propagate to the objective function. Therefore, in principle, unique identification can be enabled provided that the material model, as well as the objective function, are constructed appropriately. In case of the equilibrium gap method, this is directly possible if the material model depends linearly on the material parameters, otherwise a unique identification can not be ensured in general and also iterative procedures become necessary. However, the numerical solution of mechanical equilibrium equations will still not be required, in contrast to updating approaches. A schematic illustration of the difference between the often used FEMU-U method as a representative of updating schemes and the non-updating EGM is depicted in Fig. 1. Nevertheless, it is worth noting that the updating methods are flexible concerning the requirement of the full-field data, i.e., only a few measurements across the domain are compulsory. Whereas for the non-updating methods, full-field measurements are not only necessarily required at least in relevant domains of the structure but also with sharp spatial resolution.

In this work, regarding the points mentioned above, we propose a new methodology that engages the advantages of the non-updating methods. The basis is three-fold: first, the material model for a nonlinear anisotropic material is adapted such that the parameters appear linearly in the constitutive equations. Second, the full-field kinematics are directly inserted into the discretized equilibrium equation, representing the inhomogeneous experiment numerically. Based on the Equilibrium Gap Method, this enables the definition of a quadratic objective function in terms of differences of discrete internal and external forces. Third, a single inhomogeneous experimental setup is designed to excite all required deformation modes relevant to the material model, thus circumventing the classical approach's difficulties in performing many homogeneous tests. Two direction-dependent nonlinear material classes are considered to verify the proposed approach, starting from calendered rubber to a more complex behavior of a textile membrane. The mechanical behavior of each material is explained with the corresponding constitutive law as well as the identification of the material parameters using the classical approach. The analyses of virtual scenarios of the proposed experimental setup are presented, where the sought material parameters are predefined to serve as reference. Furthermore, the sensitivity of the method to different levels of noise added to the input displacement field is investigated. Lastly, an algorithmic treatment for the incorporation of suitable external forces is carried out.

Proposed Approach for the Identification of Parameters

In this section, major components with regard to the continuum mechanical modeling and the considered equilibrium gap method are recapitulated. Then, the proposed framework to efficiently identify stiffness-related parameters in models for hyperelasticity is presented.
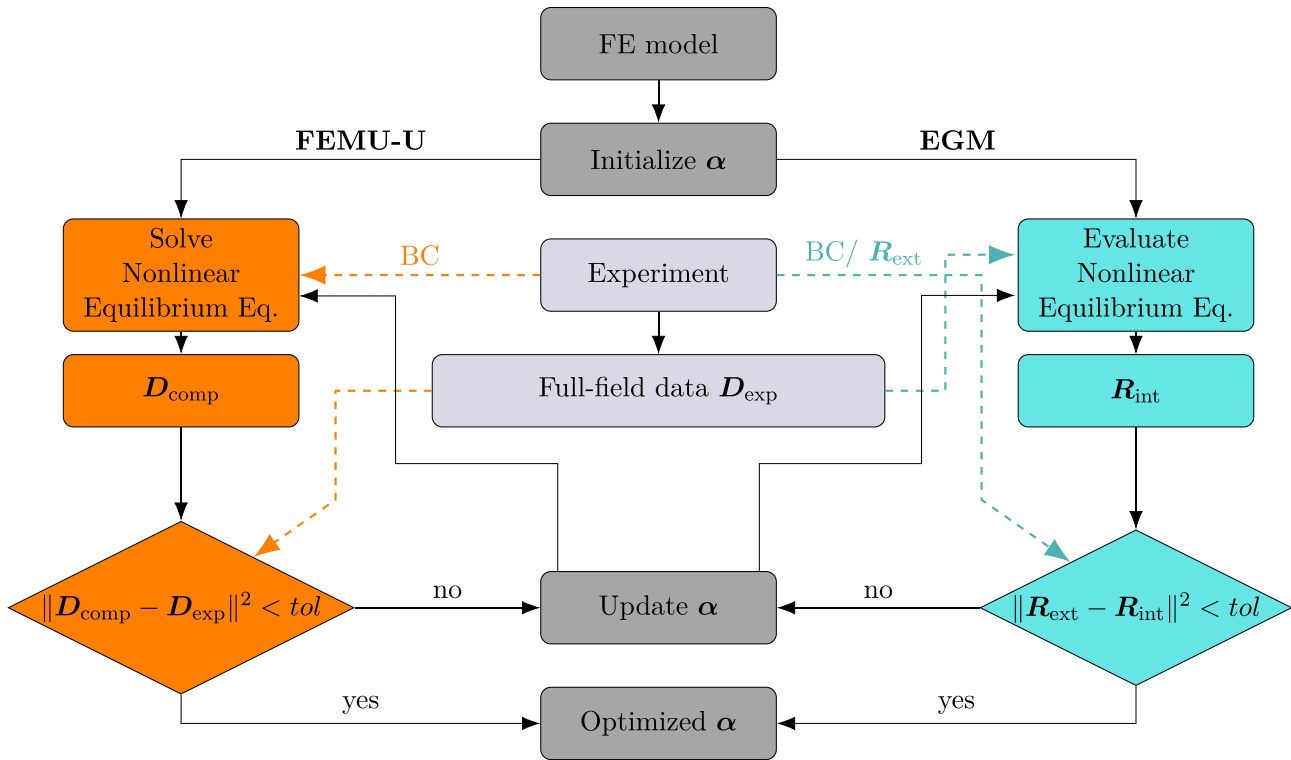
Fig. 1 Schematic comparison between the FEMU-U and EGM method

Considered Material Class and Associated Parameters

Here, we are interested in the analysis of thin, deformable materials like e.g., calendered rubber or polymeric sheets, coated textile fabrics or biomedical replacement materials. In most cases these materials are anisotropic, they allow for large deformations and often their elastic response in first loading cycles is of special interest. Therefore, we choose to consider a hyperelastic, anisotropic model for the description of these materials and the parameters appearing linearly therein to be the properties which are to be identified. A continuum mechanical basis is found in Appendix 1. The approach proposed in [9] for constructing a strain energy density function is adopted. This function is originally formulated for the simulation of textile membrane structures. It is decomposed of a series of orthotropic and transversely isotropic terms which are polyconvex. As it turns out, most formulations including the model from the literature e.g., [25] show non-converging Newton iterations in structural simulations, i.e., loss of robustness in numerical simulations of realistic structural engineering problem. The polyconvexity of the model introduced in [9] guarantees a priori the existence of a global minimizer and ensures the material stability which are very important in the context of a boundary value problem. The general structure of the strain energy density function follows

$$\psi := \alpha_1^{\text{ti}}\Phi_1^{\text{ti}} + \alpha_2^{\text{ti}}\Phi_2^{\text{ti}} + \alpha_1^{\text{orth}}\Phi_1^{\text{orth}} + \alpha_2^{\text{orth}}\Phi_2^{\text{orth}}. \qquad (1)$$

Note that this general structure $\psi = \sum_i \alpha_i \Phi_i$ with α_i denoting a stiffness-related material parameter and Φ_i a deformation function depending on suitable invariants is in line with many well-accepted polyconvex, hyperelastic models for anisotropy as e.g., [7, 26–29], and also standard isotropic models including the Neo-Hooke, Mooney-Rivlin, Yeoh and the Gent model. Herein, the transversely isotropic term Φ_i^{ti} [7] and the orthotropic term Φ_i^{orth} [29] are polyconvex functions given as follows with i referring to either direction 1 or direction 2.

$$\Phi_i^{\text{ti}} = \langle \bar{J}_{4i} - 1 \rangle^{\beta_{1i}},$$
$$\Phi_i^{\text{orth}} = \left[\frac{\tilde{J}_{4i}^{(\beta_{2i}+1)}}{(\beta_{2i}+1)\,g_i^{\beta_{2i}}} + \frac{\tilde{J}_{5i}^{(\beta_{3i}+1)}}{(\beta_{3i}+1)\,g_i^{\beta_{3i}}} - \ln(I_3^{g_i}) \right], \qquad (2)$$

The contribution of each preferred direction of the material (for instance warp and weft in textile fabrics) is captured with the term $\alpha_i^{\text{ti}}\Phi_i^{\text{ti}}$. Under the assumption that these directions can handle only tensile stresses, the corresponding energetic contribution is activated only when the stretch is greater than zero, i.e., $\bar{J}_4 > 1$, which is mathematically expressed by the use of Macaulay brackets in this term. Furthermore, the interaction between the preferred directions is

described by the term $\alpha_i^{\text{orth}}\Phi_i^{\text{orth}}$. In the case of thin materials being considered, it is worth noting that the focus is primarily on changes in shape rather than volume. Consequently, the assumption is often made that volume changes are negligible and of minor interest. As a result, the strain energy density function for these materials primarily accounts for the significant changes in shape. However, the term $\ln(I_3^{g_i})$ has a contribution in the volume deformation, where $I_3 = \det C$ is the third basic invariant of C describing the volume change. $\bar{J}_{4i} = J_{4i}I_3^{-1/3}$ is the volume preserving part of the mixed invariant $J_{4i} = \text{tr}[CM_i]$ that describes the square of the stretch in the preferred direction characterized by the normal vector a_i; $M_i = a_i \otimes a_i$ describes the second-order structural tensor which reflects the transversely isotropic material symmetry of preferred direction i. Furthermore, $\tilde{J}_{4i}$ and $\tilde{J}_{5i}$ are the mixed invariants of C and the second-order metric tensor $G_i = H_i H_i^{\text{T}}$ given as $\tilde{J}_{4i} = \text{tr}[CG_i]$ and $\tilde{J}_{5i} = \text{tr}[(\text{Cof}C)G_i]$, and $g_i := \text{tr}[G_i]$. The second-order H can be physically interpreted as a push-forward of fictional Cartesian basis $\bar{e}_i$ to the basis aligned with the material principle directions a_i as: $H : \bar{e}_i \rightarrow a_i$. For more details on the specific model, the reader is referred to the original paper [9].

In (2), the exponents β_{1i}, β_{2i}, β_{3i} and g_i are model parameters describing the degree of nonlinearity in the material response which have to be suitably chosen for a selected material class. Thereby, we fundamentally distinguish between *model* parameters, which mainly modulate the qualitative response of the model, and stiffness-related *material* parameters, which are mainly related to the quantitative response once the model parameters are chosen, i.e. once the qualitative response is defined. Note that this distinction has already been considered as part of identification procedures, see e.g., [30] or [31]. The model parameters may be selected for a particular class of materials, whereas different material parameters can then be identified for individual materials of the same class of materials. For instance, for coated textile membranes, it has been shown in [32] that fixing model parameters for one strength class of a PES-PVC material allows a very accurate representation of the stress-strain response of a range of different materials (within that class) varying in chemical composition and production technique (e.g., materials from different producers) by adapting the material parameters appropriately. Thereby, a more efficient identification procedure solely allowing for the quantification of the stiffness-related material parameters would already significantly save costs associated with the identification of material parameters required on a day-to-day basis in practice for a large number of different specific materials in one class. Furthermore, as found in [32], the stiffness-related material parameters can even be directly correlated with the strength of PES-PVC membranes, which underlines the importance of the *material* parameters.

The selection of the model parameters can either be obtained by pre-performing some classical experiments on a class of materials and e.g., applying the procedure proposed in [31]. Alternatively, an iterative identification procedure could be applied, which may consist of an external optimization of *model* parameters, where repeatedly the procedure proposed in this paper to uniquely compute *material* parameters is performed as an internal optimization problem. The resulting procedure would still only require one single experiment, however performed for a range of different specific materials of one class, and it would still significantly reduce the computational effort as the internal parameter identification does only require a very small number of solutions of the nonlinear equilibrium equations. Furthermore, the stiffness-related parameters would be uniquely computed and would allow for a quantitative interpretation. However, details of such a procedure and its analysis will be considered in future research.

For the problem at hand, in (1), the material parameters α_i^{ti} and α_i^{orth} describe the material stiffness related to the individual preferred direction and its interaction response, respectively. These are the parameters which are to be identified here. Due to the specifically chosen terms Φ_i^{ti} and Φ_i^{orth}, the strain energy density ψ is polyconvex and coercive as long as the parameter values are positive. Energy densities which are polyconvex and coercive guarantee the existence of minimizers of the total potential energy, an important requirement for any analysis based on the principle of the minimum of the total potential given in (20). Furthermore, polyconvex functions automatically fulfill the Legendre-Hadamard condition which ensures that only real wave speeds occur, cf. [33]. This is important with regard to the basic modeling assumption here that the considered material may be suitably described as a hyperelastic homogeneous body. Otherwise, in case of imaginary wave speeds, microstructures are formed whose homogenized response is only coincidentally described by the hyperelastic model and could thus, never capture reality. These mathematically and physically important issues pose constraints on the material parameters, i.e. $\alpha_i^{\text{ti}} \geq 0$ and $\alpha_i^{\text{orth}} \geq 0$ for $i = 1, 2$, which has to be suitably managed while identifying the parameters.

Objective Function Based on the Equilibrium Gap Method

The approach proposed in this paper is mainly based on a novel experimental setup in combination with extending the Equilibrium Gap Method (cf. e.g., [12]) by an iterative scheme. This method is one of the non-updating methods that makes use of full-field measurements to identify the mechanical properties of materials. It has already been successfully applied to a wide range of parameter

identification problems including homogeneous and heterogeneous elastic properties [23] or damage evolution [24]. Therefore, in this section the original EGM is briefly recapitulated and the associated objective function is given. EGM is based on extracting the constitutive law parameters which lead to the state closest to the equilibrium between discretized external forces $\boldsymbol{R}^{\text{ext}}$, known from the experiment, and internal forces $\boldsymbol{R}^{\text{int}}$, which are computed numerically for a measured displacement field. The correspondence between the internal (computed) and the external forces (measured) cannot be precise for the following reasons: the measured displacements will inevitably be subjected to errors due to the imperfect accuracy of the measurement device. Additionally, in general, material models describe the behavior of materials only approximately. Consequently, the equilibrium will be distorted. Based thereon, the residual vector $\boldsymbol{R}$, defined as the difference between the internal and the external forces, is considered the basis of the objective function to be minimized:

$$\boldsymbol{R} = \boldsymbol{R}^{\text{int}}(\boldsymbol{\alpha})\Big|_{\boldsymbol{D}^{\text{exp}}} - \boldsymbol{R}^{\text{ext}}, \tag{3}$$

Here, $\boldsymbol{\alpha}$ is the set of material parameters, and $\boldsymbol{R}^{\text{int}}$ is evaluated for the displacements $\boldsymbol{D}^{\text{exp}}$ obtained from the measurement. Since the parameters to be identified appear linear in the discrete internal forces, the objective function

$$g(\boldsymbol{\alpha}) = [\boldsymbol{R}(\boldsymbol{\alpha}) \cdot \boldsymbol{R}(\boldsymbol{\alpha})]\Big|_{\boldsymbol{D}^{\text{exp}}} \tag{4}$$

is considered to obtain a quadratic optimization problem in the parameters. Therefore, the optimization problem has a unique solution which can be obtained from any kind of gradient-based optimization strategy. The best set of parameters enabling an optimal satisfaction of mechanical equilibrium will thus be obtained by

$$\boldsymbol{\alpha} = \arg\min_{\boldsymbol{\alpha}} g(\boldsymbol{\alpha}). \tag{5}$$

In order to allow any kind of finite element software to provide the required data, we reformulate the internal forces. Remember that the strain energy density function given in (1) is linear in the material parameters, i.e.

$$\psi(\boldsymbol{\alpha}, \boldsymbol{C}(\nabla\boldsymbol{u})) = \sum_{i=1}^{N} \alpha_i \Phi_i(\boldsymbol{C}(\nabla\boldsymbol{u})), \tag{6}$$

where N is the number of terms included in the strain energy density, $\boldsymbol{\alpha} = [\alpha_1, \alpha_2, \ldots, \alpha_N]^T$ is the vector of all material parameters and Φ_i is in line with the explanation in "Considered Material Class and Associated Parameters" section. Remembering that $\boldsymbol{S} = 2\partial_{\boldsymbol{C}}\psi$, the element internal force vector can be written as

$$\boldsymbol{r}_e^{\text{int}} = \int_{\Omega_0^e} \boldsymbol{B}_e^{\text{T}}\boldsymbol{S}\mathrm{d}V = \sum_{i=1}^{N} \alpha_i \underbrace{\int_{\Omega_0^e} 2\boldsymbol{B}_e^{\text{T}}\frac{\partial\Phi_i}{\partial\boldsymbol{C}}\mathrm{d}V}_{\boldsymbol{r}_{e,i}^{\text{int}}}. \tag{7}$$

Assembling $\boldsymbol{r}_{e,i}^{\text{int}}$ over all elements yields the global counterpart

$$\boldsymbol{R}^{\text{int}} = \sum_{i=1}^{N} \alpha_i \boldsymbol{R}_i^{\text{int}} \tag{8}$$

Accordingly, the formulated objective function reads

$$g(\boldsymbol{\alpha}) = \left(\sum_{i=1}^{N} \alpha_i \boldsymbol{R}_i^{\text{int}} - \boldsymbol{R}^{\text{ext}}\right) \cdot \left(\sum_{i=1}^{N} \alpha_i \boldsymbol{R}_i^{\text{int}} - \boldsymbol{R}^{\text{ext}}\right). \tag{9}$$

Provided that the global minimum is within the range of admissible values of the material parameters, the minimum can be found by solving the system of linear equations $\partial_{\boldsymbol{\alpha}} g = \boldsymbol{0}$. The components of $\partial_{\boldsymbol{\alpha}} g$ are calculated as

$$\frac{\partial g}{\partial \alpha_j} = \frac{\partial(\boldsymbol{R} \cdot \boldsymbol{R})}{\partial \alpha_j} = 2\boldsymbol{R} \cdot \frac{\partial \boldsymbol{R}}{\partial \alpha_j} = 2\left(\sum_{i=1}^{N} \alpha_i \boldsymbol{R}_i^{\text{int}} - \boldsymbol{R}^{\text{ext}}\right) \cdot \boldsymbol{R}_j^{\text{int}}. \tag{10}$$

Herein, the discrete internal and external force vectors have to be provided by the finite element software. A straightforward and non-intrusive way to directly obtain the i-th parameter specific quantity $\boldsymbol{R}_j^{\text{int}}$ is to evaluate $\boldsymbol{R}^{\text{int}}$ by setting the corresponding α_j to 1 and the remaining ones to 0, i.e., $\alpha_j = 1$ and $\alpha_i = 0$ for $j \neq i$. The material parameters minimizing g can likewise be found based on one Newton step

$$\boldsymbol{\alpha}^{k+1} = \boldsymbol{\alpha}^k + (\boldsymbol{H}^{-1})^k \partial_{\boldsymbol{\alpha}} g^k \tag{11}$$

where $\boldsymbol{H}$ is the Hessian matrix computed as

$$H_{ij} = \frac{\partial^2 g}{\partial \alpha_i \partial \alpha_j} = 2\boldsymbol{R}_i^{\text{int}} \cdot \boldsymbol{R}_j^{\text{int}}, \tag{12}$$

where $i > 0$, $j \leq N$. This Hessian matrix can be analyzed with view to its eigenvalues in order to estimate if sufficient deformation modes have been excited in the experiment to allow for an identification of all parameters. In the case where some eigenvalues approach zero, a more sophisticated experiment should be performed. Note that if the global minimum described by $\partial_{\boldsymbol{\alpha}} g = \boldsymbol{0}$ is outside of the admissible domain, then another minimization strategy needs to be considered, where the optimizer goes along the edges of the admissible domain in an iterative procedure. However, in our case where the parameters are only restricted not to become negative, the edge of the domain would correspond to zero which would imply that the associated term in the energy function was not required.

Proposed Experimental Setup

The classical approach for the characterization of thin, anisotropic materials is to consider a large number of tests where homogeneous stress-strain fields are analyzed. The large number is required in order to obtain variations of the ratios of stresses between the preferred directions. For e.g., textile membranes, biaxial tests with varied ratios of stresses in warp and fill direction are considered [10]. To avoid such large numbers of experiments, here a non-standard experimental setup is proposed. This setup allows for the targeted activation and analysis of non-homogeneous full-field strains which already include significant variations of different stress- and/or strain ratios. The obtained inhomogeneous kinematic fields should contain all deformation modes which are addressed in the material constitutive law. The non-homogeneous displacement field is captured using Digital Image Correlations (DIC) and is then used to carry out the optimization procedure explained in "Objective Function Based on the Equilibrium Gap Method" section. The Digital Image Correlation is one of the well-established and most commonly used techniques in measuring full-field kinematics [34, 35]. Basically, it is a non-interferometric optical method through which the displacement field is acquired by comparing subregions of the images obtained before and after deformation. DIC is classified in two categories, 2D-DIC and 3D-DIC; a comprehensive comparison can be found in [36]. The 2D-DIC uses a single camera located such that its optical axis is perpendicular to the surface of interest. For this reason, 2D-DIC is restricted to the realization of two-dimensional displacements on and within the surface of a planar specimen [37]. On the other hand, the 3D-DIC is an effective tool to realize both in- and out-of-plane displacements of a surface [38]. The idea is to use two or more cameras with a range of the angle in between from 25° to 65°. Consequently, capturing the images is achieved from two or more different perspectives, after the synchronized cameras have been calibrated. In this work, the 3D-DIC is employed to measure the displacement field on the surface of the specimen. Since here we are interested in thin materials, where fluctuations of mechanical fields in thickness direction are not to be expected, the displacements measured at the top or bottom surface may already characterize the most relevant deformations in the specimen. However, the response of the material resulting from volume changes would in principle require 3D DIC measurements on both, the top and bottom surface. Since a sufficient accuracy specifically of the thickness changes using 3D DIC may be difficult for thin materials, an additional, rather standard experiment could be considered to identify the volumetric response. However, for thin materials, quantification of the volumetric response is usually not required. For instance, simulations of structures made of thin materials using membrane elements do only require two-dimensional material formulations, which can be extracted from three-dimensional models, where the response in thickness direction does not matter, i.e. the pressure can be explicitly computed from the plain stress condition, even for nonlinear material models. The associated additional hydrostatic stresses would directly enter the equilibrium gap method. In this paper, however, we analyze the real three-dimensional structure using three-dimensional finite elements to not restrict the analysis to a special case where e.g., model reduction in thickness direction is included. Therefore, we include deformation data on the top and bottom surface in our analysis to challenge the proposed approach also with respect to potential sensitivities regarding the volumetric response, although this might not even be relevant in practice.

In our approach, the specimen is on purpose subjected to loads which activate out-of-plane deformations. To induce non-homogeneous deformations with a large variety in stress ratios and in-plane shear deformation states using classical experimental machines, we propose the following experimental setup which is shown in Fig. 2. The specimen is a rectangular sheet of the investigated material with the dimensions L_1 and L_2 and the thickness t, which is clamped at the boundaries between two metal frames of width W. The load is driven perpendicular into the specimen by means of a cylindrical punch with radius r. Moreover, the machine through which the displacements are applied is able to apply rotations as well such that also a moment can be applied. Therefore, the specimen is also clamped to the cylindrical punch. Two CCD cameras are synchronized and built to capture the upper surface of the specimen during the deformation. In order to obtain full field kinematics from the data, a suitable speckle pattern is applied to the surface of the specimen before implementation. These speckles are then used as markers for measuring the displacement field using DIC. The clamps at the boundary of the specimen as well as at the inner cylindrical punch are technically realized to avoid any slip between the clamps and the specimen. Thereby, the displacements in the specimen at the edge of the clamps are geometrically known. At the boundary, the displacements are zero and at the cylindrical punch the displacements are known from the movement of the punch as part of the machine. The geometrical dimensions of the specimen have to be chosen suitably depending on the considered material to activate sufficient variations in the kinematics fields. Therefore, some a priori knowledge on the material's stiffness relations may be advantageous to directly obtain a suitable setup. For instance, if a material is particularly stiff in one direction, the length of the specimen parallel to this direction should be chosen larger to allow for sufficiently large deformations in this direction to reveal sufficient nonlinearities in the mechanical response.
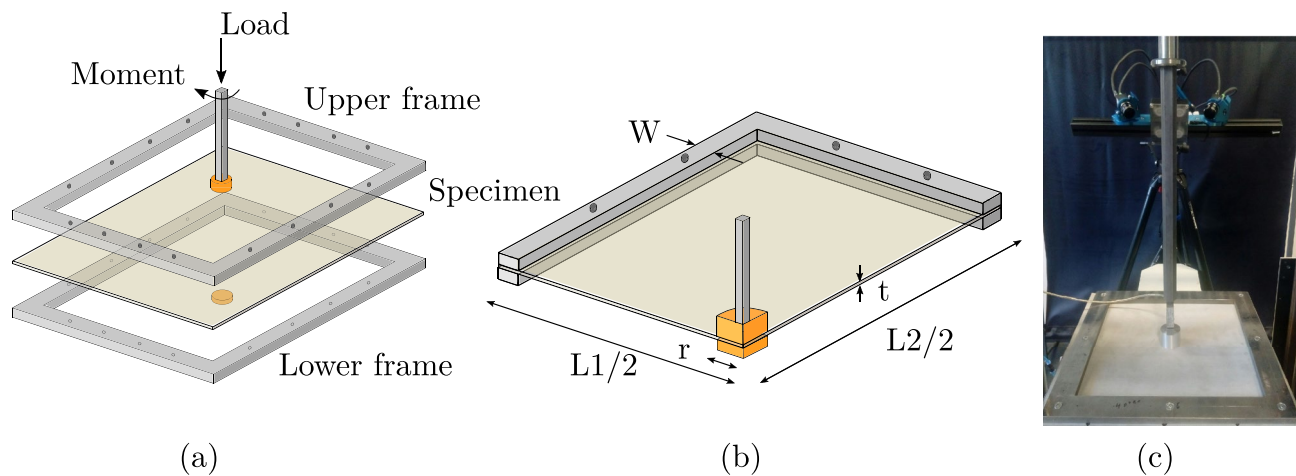
Fig. 2 Experimental setup consisting of steel frame fixed in space clamping the specimen sheet, and circular disk where the specimen is also clamped to apply the load/moment. (**a**) Schematic illustration of the disassembled setup, (**b**) schematic illustration of a quarter of the setup with the definition of the geometrical dimensions, (**c**) realization of experimental setup at the laboratory of the Chair of Continuum Mechanics at Ruhr-Universität Bochum

Although the experimental setup may appear complicated at first glance, the individual technical tasks when performing the experiment are not so much different from classical bi-axial tension tests. For the fixation of the specimen, clamping is used just as in biaxial testing, however the clamped regions differ in geometry. For the implementation of the specimen, the thin sheet is also slightly extended to allow for an implementation as a flat plane. Surely, a machine able to subject translation and rotation at the same time is required which may not be standard equipment in laboratories focusing on thin materials. On the other hand, the specimen size can be considerably smaller than for biaxial tests based on the classical cross-shaped specimens, since in our setup no homogenous state needs to be reached. Thus, the influence of the clamps on the lateral contraction response does does not need to be eliminated. Summarizing, the proposed approach represents a tradeoff between performing only one experiment at the potential cost of increased demands regarding the equipment, but fewer consumption of specimen material already for the single experiment.

An issue may be that potential instabilities may occur in the sense that for certain loading protocols, e.g., when applying too large rotations relative to the applied translations, wrinkles may appear. This can, however, be easily avoided by either performing pre-tests (as usually done in any kind of experiments) or by simply applying the translation first and then adding rotations until wrinkles appear.

Extended Iterative Scheme for Unknown Distribution of External Forces

From the DIC measurements, only information regarding the kindematics in the specimen can be obtained. However, for the identification procedure using the equilibrium gap method described in "Objective Function Based on the Equilibrium Gap Method" section, at least at some part of the boundary which is connected to the region of measured kinematics, the external forces R^{ext} need to be known as well. Otherwise, the identification problem is ill-posed. Whereas a measurement of external forces at the outer boundary of the specimen would be technically demanding, at least the resultants of the external forces at the edge to the cylindrical punch are known from the machine. Therefore, we choose to consider this edge to be part of the problem and exclude the outer boundary from the identification procedure. Although the resultants are known from the machine, the specific distribution of external forces along the punch needs to be suitably estimated. The anisotropy of the investigated materials leads to an inhomogeneous distribution of the vertical, the tangential, and the radial components of the external force vector resulting from the applied force and moment, i.e. R^{ext}_z, R^{ext}_t, and R^{ext}_r. Therefore, an iterative scheme is proposed here to find an appropriate estimation for the correct distribution of the reaction forces. The according algorithmic treatment is given in the algorithmic box 1.

Algorithm 1 Iterative scheme for the estimation of the distribution of external forces.

1: Initialization: Assume a uniform distribution of R_z^{ext} and R_t^{ext}, assume $R_r^{\text{ext}} = 0$
2: Perform EGM to compute $\boldsymbol{\alpha}^k = \boldsymbol{\alpha}^0$
3: Solve forward BVP using $\boldsymbol{\alpha}^k$ and compute distribution of $R_z^{\text{ext},k+1}$, $R_t^{\text{ext},k+1}$ and $R_r^{\text{ext},k+1}$
4: Perform EGM to compute $\boldsymbol{\alpha}^{k+1}$
5: Compute minimum relative error $\xi = \min_i \left[\dfrac{\alpha_i^{k+1} - \alpha_i^k}{\alpha_i^k} \right]$
6: **IF** $\xi > tol$ **THEN** $k \Leftarrow k+1$ and go to 3

The iterative scheme starts from an initial guess for the distribution of the components R_z^{ext} and R_t^{ext} which are assumed to be uniform and their resultants to match with the force and moment applied by the machine. Furthermore, a zero initial guess is considered for the radial forces R_r^{ext} since they or their resultant are not experimentally known. The EGM is carried out thereon, and a set of material parameters corresponding to the initial guess of the distribution of forces is determined. Solving the forward problem for the obtained parameters will give the first approximation of the distribution of reaction forces, which will then be used for the EGM, and a new set of material parameters will be obtained. This procedure is then repeated until a convergence criterion is fulfilled, i.e. $\xi < tol$ is detected for a predefined tolerance tol. Herein, ξ is defined as the minimum value over all relative deviations between the parameter α_i^{k+1} obtained at the current iteration $k+1$ and those obtained at the previous iteration α_i^k, $i \in 1 \dots N$. The whole parameter identification procedure consists then of the following steps:

1. Define suitable size of specimen and load protocol for force and moment
2. Implement specimen into the clamps
3. Perform experiment by applying load/moment protocol
4. Measure full-field kinematics using 3D-DIC at each deformed state
5. Perform Algorithm 1 to identify parameters

Note that it is convenient to design a technical realization of the clamp in the disk which avoids a significant change of specimen thickness here. Thereby, the deformations in the disk and at the boundary are indeed known. Otherwise the related thickness change could have a significant impact on the boundary forces at the disk. Then, this influence could be taken into account within the iterative scheme by incorporating volume elements which discretize the real thickness of the specimen in the disk to obtain a more realistic estimate of the distributions of boundary forces. This technical complication would only relate to the solution of the forward BVP (step 3 in Algorithm 1), not the identification procedure in step 2, where still membrane elements may conveniently be used.

Analysis of Proposed Method

In this section, the proposed method for the parameter adjustment is analyzed based on virtual experimental data. This virtual data is obtained from numerical simulation of the new experimental setup using parameter values which have been obtained based on classical parameter adjustment. Thereby, the parameters obtained from the classical approach serve as reference solution which allows a suitable assessment of the proposed method's performance. Clearly, a mechanical response obtained from applying parameters identified with the proposed approach, which agrees well with the reference data, shows that the identification method can successfully be applied. A less accurate representation, in this context, does not mean that the model is not appropriate as the model itself is used to produce the reference data. To make sure that realistic scenarios are considered in the analysis, the individual results are also compared with real experimental data. As will be shown in this section, different variations of experimental setups in terms of loading protocols, specimen fixations, or measurement accuracy are differently suited for the purpose of an accurate parameter identification. By including different levels of noise mimicking the experimental variation, the sensitivity of the proposed method can be assessed quantitatively in a controlled environment. Furthermore, by application of parameters and models well describing a real material response we can make sure that our analysis is not purely academic.

Classical Adjustment to Experiments as Reference

Usually, the material parameters are obtained by fitting the material model to experimental stress-strain data obtained from several uni- and biaxial tests with varying ratio of loads in the two main anisotropy directions. For this purpose a proper objective function is formulated as a least square error between measured and computed quantities. These quantities are the strains and/or stresses resulting from prescribed forces and/or displacements. In order to obtain suitable reference material parameters, we follow the identification procedure detailed in [39]. In order to show that the proposed method is not restricted to a specific material, we consider two different orthotropic, thin materials: calendered rubber and coated woven fabric. Since we also want to analyze the proposed method for different levels of complexities of parameter identification problems, we on purpose start with a simplified formulation for calendered rubber consisting of two orthotropic terms and then analyze a coated fiber fabric modeled by two transversely and two orthotropic terms. Note that the
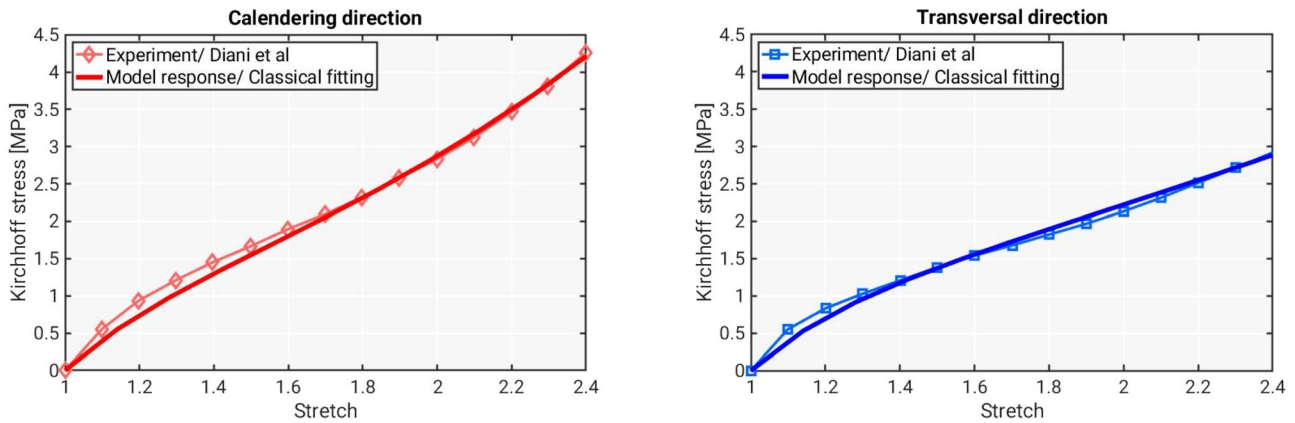
Fig. 3 Experimental data extracted from [4] and model response of a calendered rubber sheet under uniaxial stretching applied in the calendering and the transverse direction. Here, Kirchhoff stresses $J\sigma$ in MPa are plotted versus stretch l/l_0 with l_0 indicating the undeformed specimen length

models considered here should be interpreted as prototype models for the feasibility study of our approach. There are many alternative formulations for calendered rubber and coated woven fabrics in the literature which may represent experimental data more accurately.

Calendered Rubber Calendering is the process of manufacturing webs, sheets, and films from polymer melts. The raw material is heated and then subjected to pressure by feeding it between two cylindrical rollers rotating in opposite directions. Thereby, orthotropic material properties are obtained. Due to the process' ability to precisely adjust the product thickness, calendering lines are nowadays used to produce many products, aside from rubber, such as thermoplastic films, sheets, and coatings.

Here, we focus on calendered rubber as investigated in [4], namely, calendered rubber filled with silica particles. There, an orthotropic material response showing large deformations was concluded, and thus, the experimental data provided therein is considered here, cf. Fig. 3.

Due to the restricted experimental data only consisting of uniaxial tests, we choose a simplified material model only consisting of two orthotropic terms and thus, the strain energy density function becomes

$$\psi := \alpha_c \Phi_c^{orth} + \alpha_t \Phi_t^{orth} , \tag{13}$$

with indices c and t referring to the calendering direction and the transverse direction. Herein, the orthotropic functions follow the ones defined in (2). Note that other models able to describe the behavior of calendered rubber more appropriately can be found in the literature, see e.g., [27]. As can be seen, applying a classical fitting procedure leads to a good agreement of the considered model with the experiments, see Fig. 3, and thus, to a suitable reference set of parameters presented in Table 1.

Coated woven fabric Two woven yarn families made of glas are interlaced and covered with a PTFE coating material to form the thin structure of a textile fabric. Its high tensile strength, durability, and fire resistance, along with a distinctive high strength-to-weight ratio make this textile fabric attractive in many engineering applications such as enclosing wide spans of roofs, air-halls, and facades. The yarns in the direction of production are the warp yarns, while the ones running in the transverse direction are the fill yarns. For modeling and characterization purposes, it is suggested as a standard procedure to study the deformation of textile membranes in biaxial tests with varying load ratios in warp and fill directions. The mechanical behavior of the textile membrane under tensile loading is highly nonlinear and anisotropic. The effect of 'crimp interchange', i.e., the interaction between the yarns, is the main reason for the

Table 1 Parameters of the proposed strain energy density function obtained from classical fitting of the model response to experimental data on calendered rubber and woven coated fabric

| i | Transversal isotropic | | Orthotropic | | | |
	α	β_1	α	β_2	β_3	G
c	–	–	2.272	10.0226	0	diag[0.4, 0.296, 2.316]
t	–	–	131.726	5.6125	0.5635	diag[0, 0.008, 0.5]
Warp	3039400	3.875	1.1719	0	34.985	diag[1, 1.36, 1.75]
Fill	47259	6.6016	2.023	35	0	diag[1.41, 1, 0]

fabrics' non-linearity. Many studies have been carried out to construct suitable mathematical models to describe the saturated, elastic behavior of textile membranes starting from orthotropic linear elastic models, e.g., [40–42] to nonlinear anisotropic models, e.g., [9, 25]. According to the Japanese guideline MSAJ/M-02.1995, the load profile for the characterization of the textile membrane consists of two monoaxial stress ratios (warp:fill) 1:0 and 0:1 and three biaxial stress ratios 1:1, 1:2, and 2:1. These tests have been performed at Essen Laboratory of Lightweight Structures (ELLF), University of Duisburg-Essen. In line with [9], we consider the strain energy density

$$\psi := \alpha_{\text{warp}}^{\text{ti}} \Phi_{\text{warp}}^{\text{ti}} + \alpha_{\text{fill}}^{\text{ti}} \Phi_{\text{fill}}^{\text{ti}} + \alpha_{\text{warp}}^{\text{orth}} \Phi_{\text{warp}}^{\text{orth}} + \alpha_{\text{fill}}^{\text{orth}} \Phi_{\text{fill}}^{\text{orth}} \quad (14)$$

where the individual functions follow (2). Although the model of [25] is able to more accurately represent the non-linear, anisotropic response of multiple biaxial tests with varying load ratios simultaneously and even the lateral contractions under uniaxial loading, its lack of polyconvexity leads to several issues including the loss of material stability. In the comparative study in [9] it has been shown that an unphysical response is obtained at moderate strains and significant numerical issues arise making structural simulations difficult. These issues render the practical applicability of non-polyconvex models problematic. Since the polyconvex model of [9] also allows a quite decent representation of

multiple experiments, this model is considered here. The material model has been fitted to the five tests simultaneously and the parameters given in Table 1 were obtained. The corresponding stress-strain curves are depicted in Fig. 4. As can be seen, the model matches well with the experiments and thus, a relevant reference setting for the analysis of the new method is obtained.

Note that the model parameters (β_{1i}, β_{2i}, β_{3i} and g_i) are kept fixed, and the material parameters appearing linearly in the strain energy density function (α_i) are investigated using the approach explained in "Objective Function Based on the Equilibrium Gap Method" section.

Study of the Proposed Approach - Impact of Measurement Noise

As a first analysis for the general applicability of the approach described in "Objective Function Based on the Equilibrium Gap Method" section in combination with the new experiment from "Proposed Experimental Setup" section, we consider the displacements obtained from a finite element (FE) analysis of the experimental problem as virtual experimental input to the identification procedure. In order to render this setup to be realistic, different levels of noise mimicking the variations in the displacement fields in real experiments are applied to the displacement field. Then,
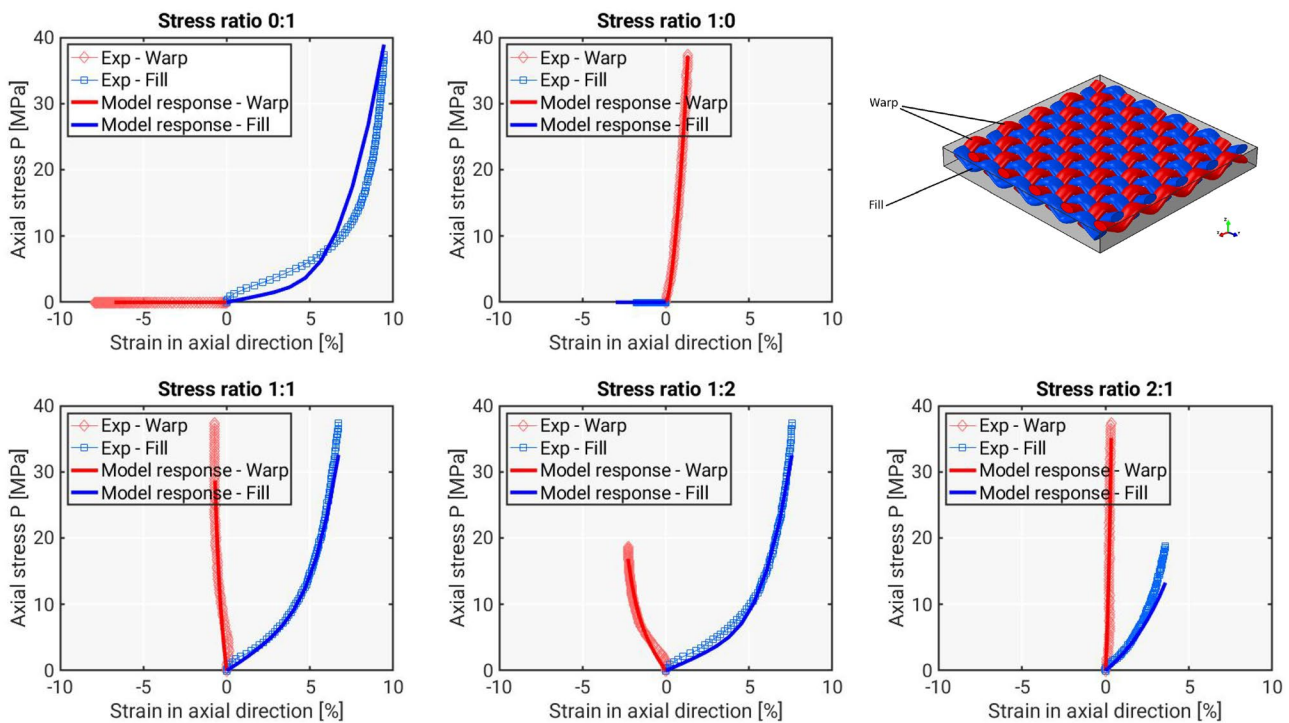
Fig. 4 Experimental data and model response for the coated woven fabric for five different stress ratios. Here, first Piola-Kirchhoff stresses are plotted versus strains in %
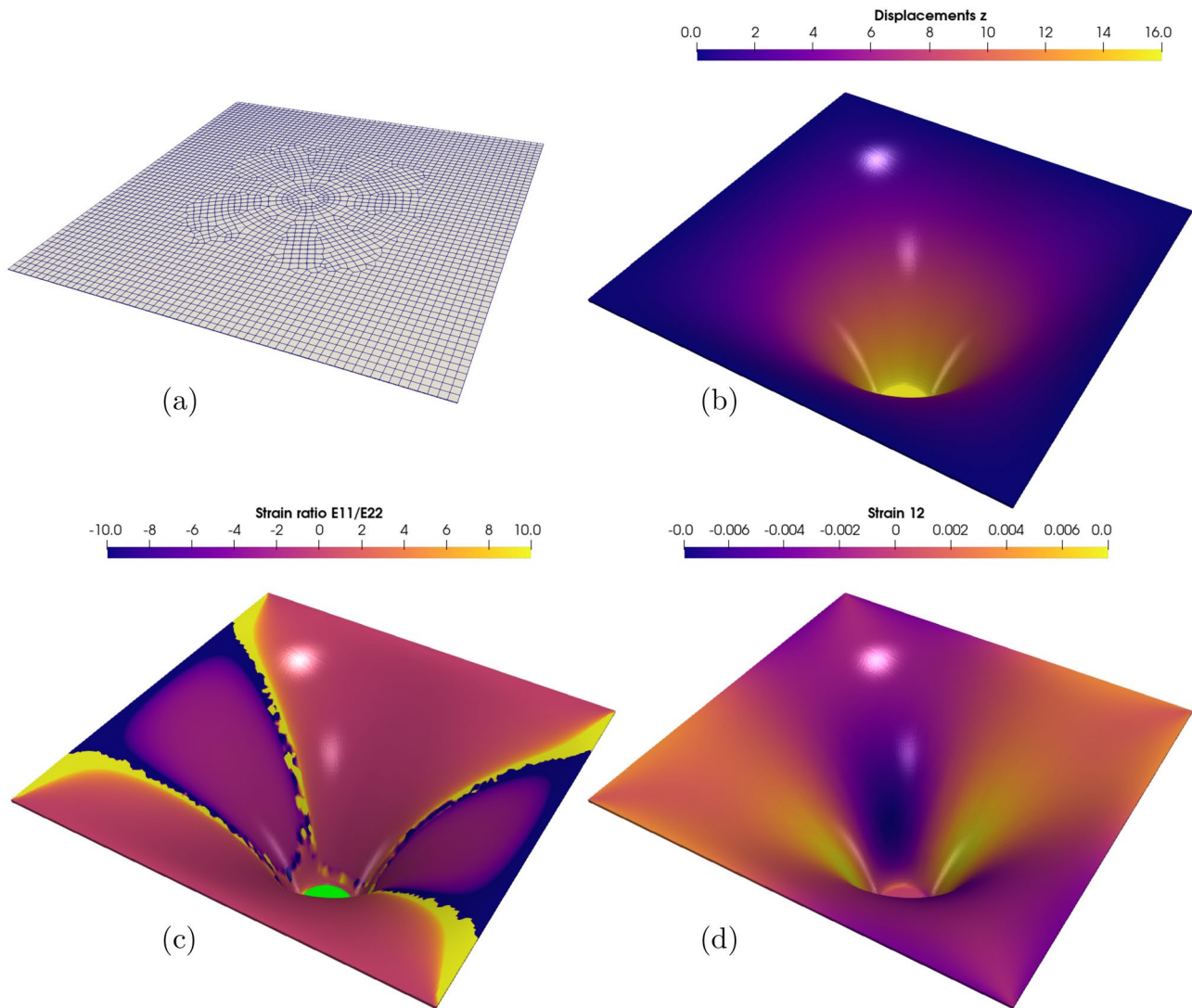
Fig. 5 Computational model serving as reference (virtual experimental) data: (**a**) the discretized undeformed structure, (**b**) a characteristic scenario of the deformed structure with displacements in pushing direction in mm as contour plot, (**c**) the ratio E_{11}/E_{22} (the green color indicates the area where no ratio has been computed due to the zero strains resulting from pure rigid body motion), and (**d**) the shear strain component E_{12}. Clearly, a significant variation of strain ratios and shear strains is induced in the sheet from to the experimental setup

the identification procedure is performed and its results are compared for the different levels of noise. For the analysis, two different in-silico loading protocols (LPs) are considered: vertical displacements of the punch (LP1) and vertical displacements combined with rotations (LP2). The FE analysis, being the forward problem, is solved using the open-source finite element software FEAP, where the material parameters are prescribed to be the ones obtained using the classical identification procedure explained in "Classical Adjustment to Experiments as Reference" section. The FE model for the proposed experimental setup is shown in Fig. 5(a). The structure is discretized by a grid consisting of 8-node brick elements with tri-linear shape functions for the displacements. The specimen is clamped at the edges

in all directions according to the experimental design. The cylindrical punch itself, through which the displacements are applied to the sheet, has not been modeled. Instead, the cylindrical region in the center of the sheet of 40 mm diameter is considered rigid (due to the clamp), and the displacements resulting from pushing and turning the punch are applied directly to the nodes within this region. The nonlinear boundary value problem is then solved by using the Newton–Raphson scheme, where the complete load is divided into a number of 500 load steps where in each load step, a Newton iteration is performed until the norm of displacement increments falls below a predefined tolerance. A representative illustration of the deformed structure is shown in Fig. 5(b). There, a vertical displacement of the center

region of 16 mm downwards has been considered; here, no rotation of the center region has been applied. As can be seen, a large variety of strain ratios and the shear strains is obtained, as depicted in Figs. 5(c) and (d). In contrast to such numerical results, real displacement fields captured by DIC are subject to noise due to multiple reasons, including an imperfect accuracy of the optical device, a potential lack of light intensity, an imperfect speckle pattern, etc. This noise was found in 2006 to result in a relative error of the displacements obtained from DIC of 0.01% − 0.05% [43]. To further justify the choice of this noise level for our analysis, the DIC system's accuracy at the Continuum Mechanics laboratory at Ruhr University Bochum has been assessed by a simple experiment, which is described in Appendix 2. Results show that the measured displacement field is subject to a relative error ranging from 0.01% to approx. 0.03%. Therefore, adopting a noise range of 0.01% − 0.05% can be considered sufficiently conservative. Since a significant part of the analysis showed a relative error around 0.01%, the results presented in this section associated with an error of 0.01% may be reached in reality if sufficient effort is invested on the quality of the measurement. Considering that measurement accuracy will increase in the future, rather low levels of noise can be anticipated. Based thereon, the virtual experimental displacements as input to the EGM, which are here computed from the FE simulations, are corrupted by the modification

$$D_j^{\text{noi}} = (1 + \Theta_j)D_j, \quad j = 1, \dots n_{\text{dof}}, \tag{15}$$

where $\boldsymbol{D}^{\text{noi}}$ and $\boldsymbol{D}$ are the global vectors of the generated discrete noisy displacements and the discrete computed displacements respectively; n_{dof} is the number of global degrees of freedom. $\boldsymbol{\theta}$ is a vector of Gaussian distributed random scalar numbers with zero mean μ and standard deviation σ so that 95% of the sampled variables are within the confidence interval of $\pm 0.01\%$ and $\pm 0.05\%$.

Moreover, in order to eliminate the need to measure the reaction forces at the clamped edges, the corresponding nodes have been excluded from the optimization procedure. Furthermore, due to the symmetry, only half of the specimen is included in the analysis. The nodal displacements D_j obtained from these calculations are then considered as raw data representing experimental data which enters the identification procedure after application of noise. It is important to highlight that since the specimen is discretized with one brick element through the thickness, the displacements of the nodes positioned on both the upper as well as the lower surface of the specimen are included in the analysis. In this case, the thickness stretches are taken into account, thereby addressing the impact of volume changes on the identified parameters. The nodal reaction forces at the circular center region of the punch are stored at the end of each of the

M solution load steps. Consequently, the objective function defined in (4) has to be added up for the considered load steps and thus, it reads

$$g(\boldsymbol{\alpha}) = \sum_{m=1}^{M} g_m(\boldsymbol{\alpha}), \tag{16}$$

where $g_m(\boldsymbol{\alpha})$ is the objective function evaluated for the displacement field obtained at load step m. The parameter values resulting from minimizing this objective function can then be compared with the predefined reference values, which were used to obtain the virtual experimental data. For their quantitative comparison, the relative error measure

$$\eta(\alpha_i) := \frac{\alpha_i^{\text{ide}} - \alpha_i^{\text{pre}}}{\alpha_i^{\text{pre}}} \tag{17}$$

is considered for each parameter α_i. Herein, α_i^{ide} and α_i^{pre} are the identified and the predefined parameters, respectively. The analysis for the calendered rubber and the coated woven fabric specimen is described in the following.

Calendered rubber

The calendered rubber specimen investigated in the experimental setup explained in "Proposed Experimental Setup" section is of dimensions $L \times L \times t = 300 \times 300 \times 2 \text{ mm}^3$. A preliminary analysis has been conducted in Appendix 3 in order to investigate the effect of the number of the recorded loading states M included in the objective function on the identified parameters. This investigation has been done considering loading protocol 1 (LP1) with examining a number of 50, 20 and 10 states along the deformation. It can be noted from the relative error plotted in Table 4 that larger numbers of the considered deformation states lead to larger errors in the values of the identified parameters. Based on this observation, the identification results presented in the remainder of the paper are obtained by considering $M = 10$ states along the deformation process. Now, the loading protocol 2 (LP2) with 10 mm vertical displacements combined with 45° torsion is analyzed. The resulting relative error is reported in Table 2 for a noise range of $\pm 0.01\%$ and $\pm 0.05\%$. A maximal

Table 2 Relative error of the identified parameters for the calendered rubber, where loading protocol 2 for different noise ranges in analyzed. LP2 refers to applying vertical displacements combined with rotations. The impact of the resulting parameters on the material behavior is shown in Fig. 6

| Scenario	$\eta(\alpha_{\text{c}})$	$\eta(\alpha_{\text{t}})$
LP2, noise range $\pm 0.01\%$	0.004	0.001
LP2, noise range $\pm 0.05\%$	0.04	0.03
LP2, noise range $\pm 0.01\%$, Iterative EGM	0.004	0.001
LP2, noise range $\pm 0.05\%$, Iterative EGM	0.043	0.032

value of 0.4% and 4%, respectively, can be observed, which is significantly lower than for loading protocol 1 (check Appendix 3, where the relative error is 33% for noise range 0.01%). This indicates the necessity to also include torsion to the experiment in order to increase the amount of activated deformation modes. Accordingly, the stress-strain response using the identified parameters in uniaxial tension agrees now very well with the real experiments, see Fig. 6.
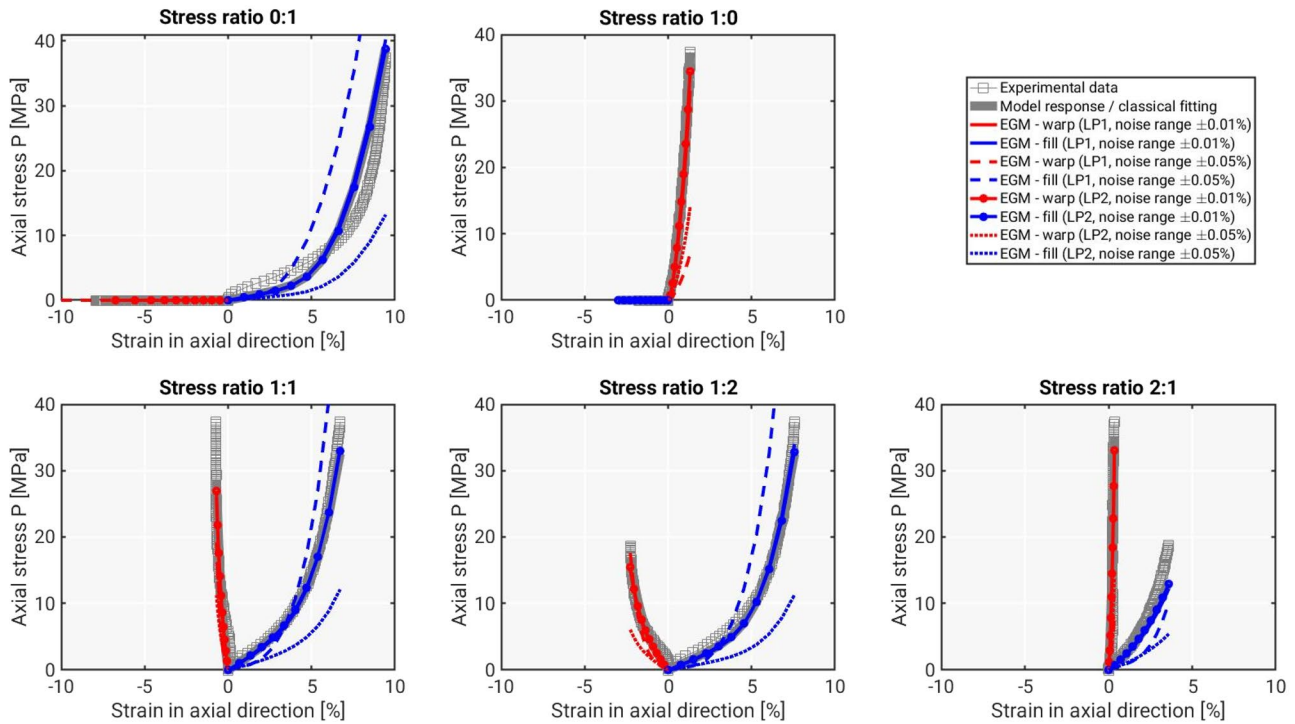
Coated woven fabric

The considered specimen made from coated woven fabric is of dimensions $L \times L \times t = 300 \times 300 \times 0.53 \text{ mm}^3$. Considering loading protocol 1 (LP1) with a total amount of applied vertical displacements of 17 mm, the material parameters are obtained with a maximal relative error of 15% for noise range 0.01%, see Table 3. However, for noise range 0.05% the parameters are obtained with relative error up to 84% with exceeding 100% for the single parameter associated with the transversely isotropic term in the fill direction. Figure 7 shows the resulting discrepancy between the model response obtained from EGM (dashed lines) and the real experimental data. This discrepancy can be explained under the following premise: the warp direction is stiff, and it requires approximately 2% strain to reach the ultimate principal stress, while the fill direction is soft requiring strains of about $7-9\%$ to reach the ultimate principal stress. For LP1, the warp direction reaches the ultimate stress while the fill direction does not exceed half the value, see Fig. 8. Hence, a more suitable loading protocol is needed to excite the nonlinearity of the fill direction and to assure at the same time that ultimate stresses are not exceeded in warp direction. Considering loading protocol 2 (LP2) with vertical displacements of 10 mm, 3° torsion, noise range 0.01%, the maximum relative

error is 7%, see Table 3. Accordingly, the model response agrees much better with the experimental data compared to LP1, see Fig. 7. For higher (and admittedly unrealistically large) noise 0.05%, the relative maximum error is 60%, with the relative error on the parameter associated with the transversely isotropic term of 74% (see Table 3), leading to a discrepancy between the model response and the experimental data (see dotted lines in Fig. 7). This means, that the fill direction is still sensitive to noisy displacements which is most probably due to the fact that the fill direction is not sufficiently stimulated.

Therefore, there is still room to improve the quality of identified parameters by using different boundary conditions on the specimen motivated by the strong anisotropy of the coated woven fabric. By introducing a third loading protocol LP3, where the clamps supporting the yarns in the warp direction are released, the specimen stiffness in warp direction is significantly reduced. This allows for the application of much larger vertical displacements before rupture (here 50 mm) and a torsion of 4°. Based thereon, the relative maximum error results in 1.5% when a noise range of $\pm0.01\%$ is added to the displacement field; for noise range $\pm0.05\%$, the maximum error is 47% (see Table 3). This shows that significant improvements can be achieved from this modified loading protocol. However, further improvements can be achieved by incorporating the nonlinear characteristics of the material response more directly in the EGM approach. In fact, the response of the coated woven fabric under combined punching and torsional loading is increasingly stiff as the deformation progresses. Therefore, to better capture the nonlinear response, an emphasis can be put on the later part of the deformation process as the unloaded configuration is a priori included. To this end, the last ten load steps out of
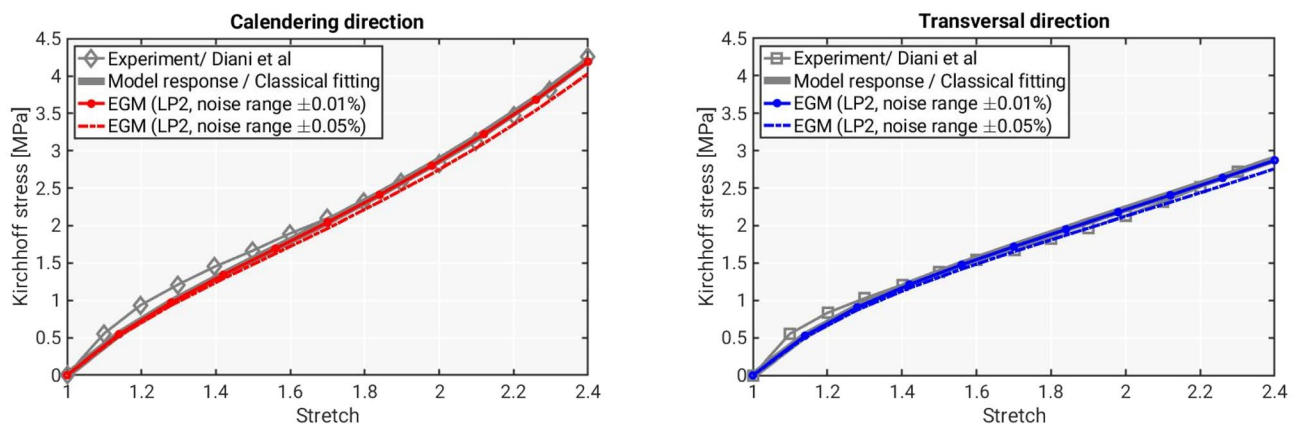
Fig. 6 Calendered rubber specimen under uniaxial tension: comparison of experimental data and model response evaluated for sets of parameters obtained by including different noise ranges added to the displacement field and considering load protocol LP2, where vertical displacements and rotations are applied in the experimental setup. As can be seen, an accurate representation of the classical experiment is obtained when identifying the parameters based on LP2

Fig. 7 Coated woven fabric specimen under uniaxial tension and biaxial tests: Comparison of experimental data and model responses evaluated for sets of parameters obtained from EGM for LP1 and LP2 and different noise ranges added to the displacement field. Note that the curves for the lower noise range match almost perfectly with the reference response obtained from the classical fit

in total 500 load steps are used as an input to the EGM scheme, instead of considering ten states equally distributed along the whole deformation. As a consequence, the maximum relative error in the identification is is reduced to just a few percent when noise range $\pm0.01\%$ is considered. If the noise range of $\pm0.05\%$ is included, the maximum error results in 23% (see Table 3). Correspondingly, a strong improvement in the simulated stress-strain behavior

is recognized in Fig. 9 replicating much better the behavior under classical uniaxial and biaxial tests.

Analysis Based on the Iterative EGM

The above results show that the proposed approach works quite accurately when choosing appropriate loading protocols and deformation states. However, the results
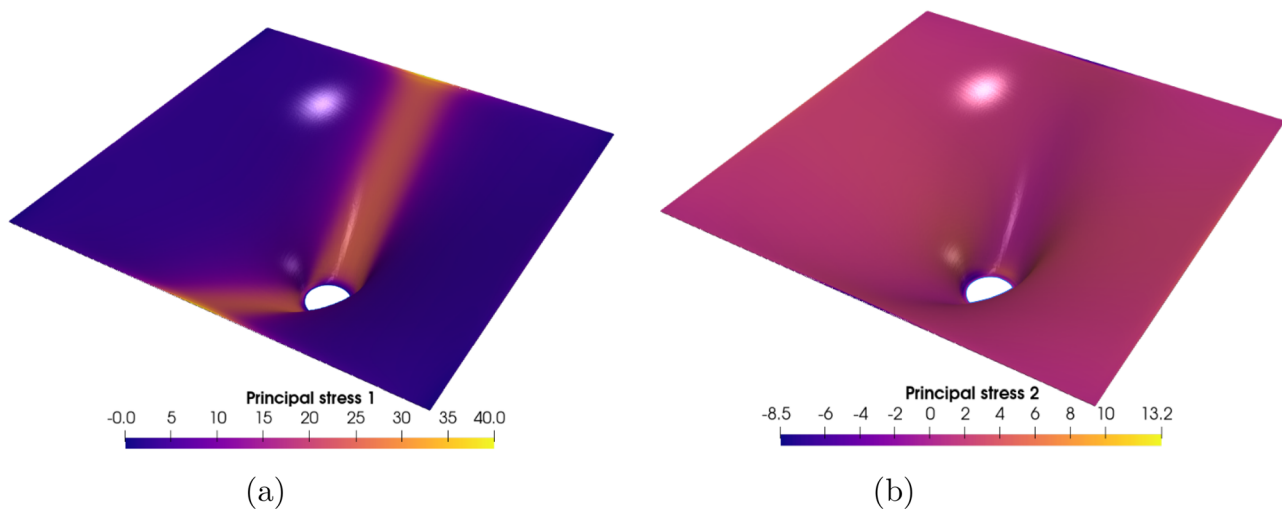
Fig. 8 Principal stresses in coated fabric for LP1 in (**a**) warp direction and (**b**) fill direction

Table 3 Relative error of the identified parameters for the coated woven fabric for different scenarios, where varying load protocols, noise ranges, and boundary conditions are analyzed. LP1 refers to the case where purely vertical displacements are considered and LP2

to additionally applying rotations. While LP3 refers to applying displacements and rotations on the specimen after releasing the clamp in warp direction. The impact of the resulting parameters on the material behavior is shown in Figs. 7 and 9

Scenario	$\eta(\alpha_{warp}^{ti})$	$\eta(\alpha_{fill}^{ti})$	$\eta(\alpha_{warp}^{orth})$	$\eta(\alpha_{fill}^{orth})$
LP1, noise range ±0.01%	0.15	0.11	0.14	0.10
LP1, noise range ±0.05%	0.82	> 1	0.84	0.55
LP2, noise range ±0.01%	0.07	0.05	0.06	0.06
LP2, noise range ±0.05%	0.60	0.74	0.62	0.59
LP3, noise range ±0.01%	0.015	0.01	0.01	0.005
LP3, noise range ±0.05%	0.47	0.43	0.46	0.18
LP3, noise range ±0.01%, last loading states	0.014	0.007	0.008	0.004
LP3, noise range ±0.05%, last loading states	0.23	0.17	0.19	0.08
LP3, noise range ±0.01%, Iterative EGM	0.02	0.01	0.01	0.008
LP3, noise range ±0.05%, Iterative EGM	0.3	0.21	0.23	0.11

obtained so far were achieved by prescribing the boundary forces at the center disk which were obtained from the initial simulation serving as reference scenario (virtual experiment). In real experiments, however, the force distribution at the boundary of the center disk is not known, although the resultant forces are known from the machine. Then the iterative scheme proposed in "Extended Iterative Scheme for Unknown Distribution of External Forces" section can be applied. Therefore, this approach is now investigated, again for the two material classes.

Calendered rubber

The analysis of the iterative scheme is carried out for loading protocol 2 (LP2). The distribution of the vertical, radial, and tangential components of the reaction forces, i.e. R_z, R_r, and R_t, on the circular disk as obtained by solving the forward problem is shown in Fig. 10. The iterative EGM scheme explained in "Extended Iterative Scheme for Unknown Distribution of External Forces" section is now applied for the identification of the material parameters.
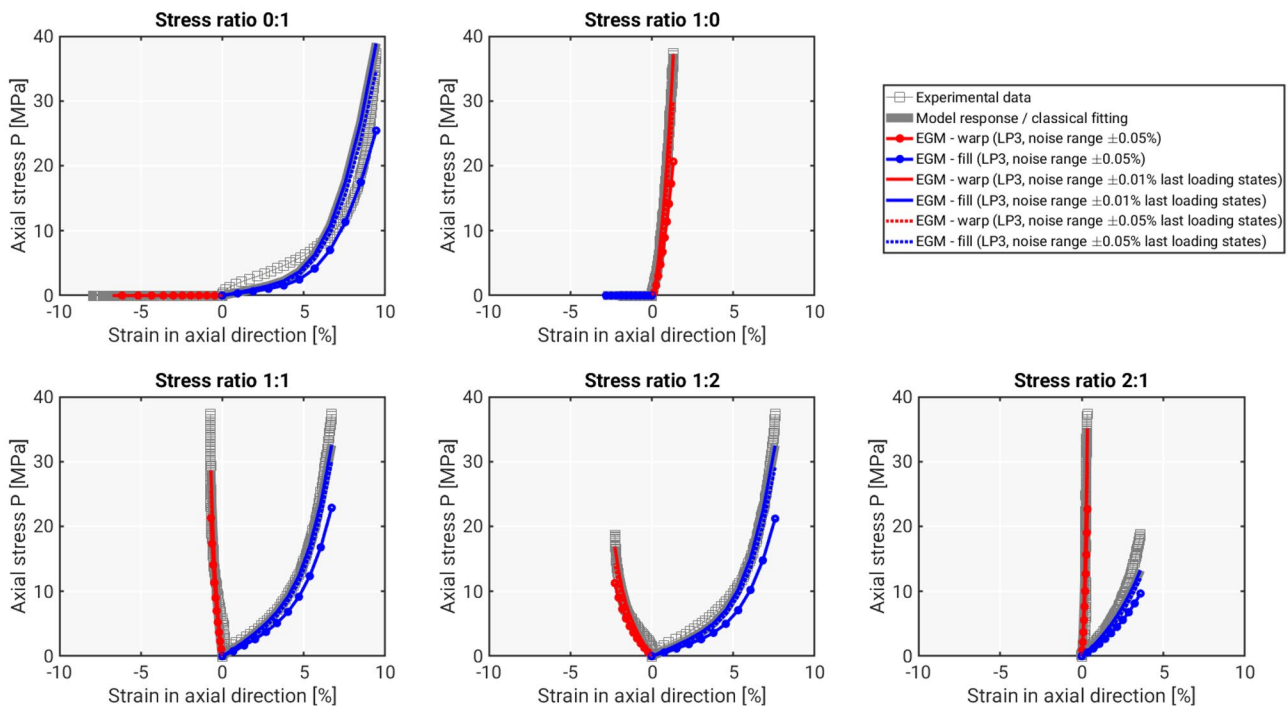
Fig. 9 Coated woven fabric specimen under uniaxial tension and biaxial tests: Comparison of experimental data and model responses evaluated for sets of parameters obtained from EGM considering new BC for loading protocol 3 and different noise ranges added to the displacement field. Note that the curves obtained from considering only the last loading states lie on top of each other for the lower and higher noise ranges. An accurate representation of the real experimental data can be achieved by the model when using the proposed approach
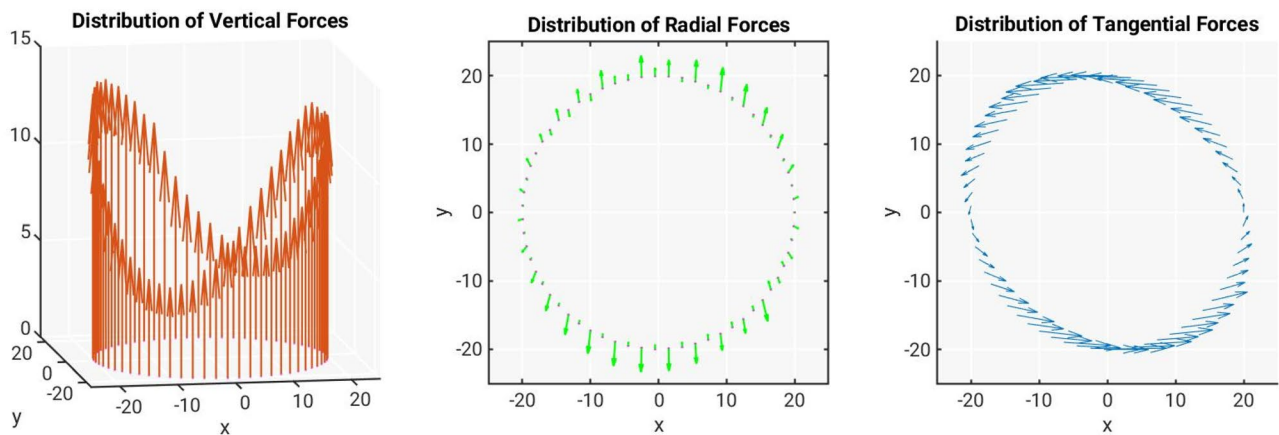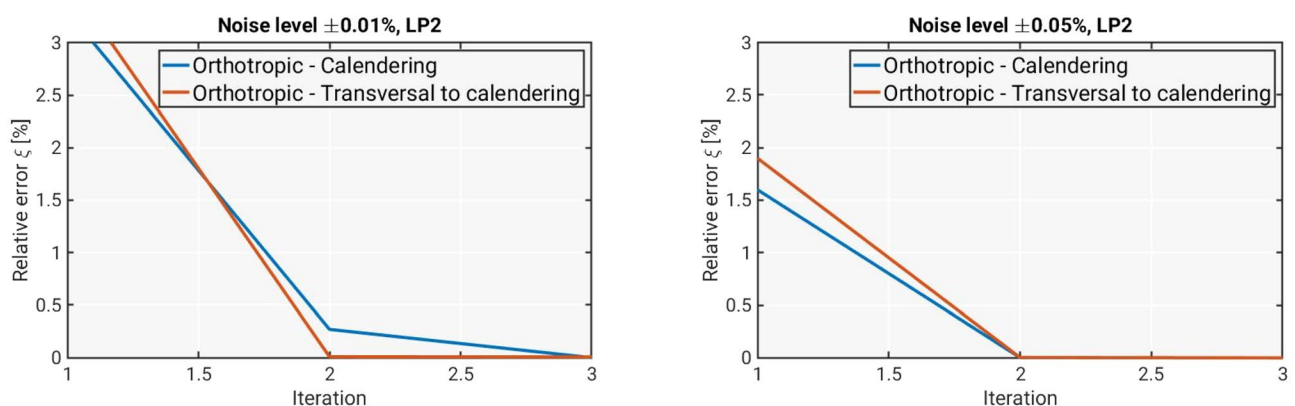
Fig. 10 Distribution of the reaction forces on the cylindrical punch considering loading protocol 2 (LP2) applied to the calendered rubber specimen. The radial forces are almost zero (scaled 5 times in the corresponding plot) and the tangential forces are almost uniformly distributed along the circumferential position (scaled with the factor 0.2 in the corresponding plot)

As initial guess, a uniform distribution of vertical and tangential forces as well as zero radial forces are considered. Based thereon, the relative error defined in "Extended Iterative Scheme for Unknown Distribution of External Forces" section is plotted along the iterations in Fig. 11. As can be seen, only three iterations of solving the forward problem are needed to correct the reaction forces' distribution and determine the optimal set of parameters. This number of iterations was achieved for both cases of noise ranges, i.e. ±0.01% or ±0.05%. Similar to "Study of the Proposed Approach - Impact of Measurement Noise" section, the quality of the parameters obtained using the iterative EGM scheme is assessed by computing the relative error to the prescribed values for each parameter individually. The results are presented in Table 2 for noise ranges 0.01% and 0.05%. As can be seen, the relative errors obtained from the iterative EGM scheme (where the force

distributions are iteratively updated) are quite similar to the ones obtained from prescribing the exact distribution of forces.
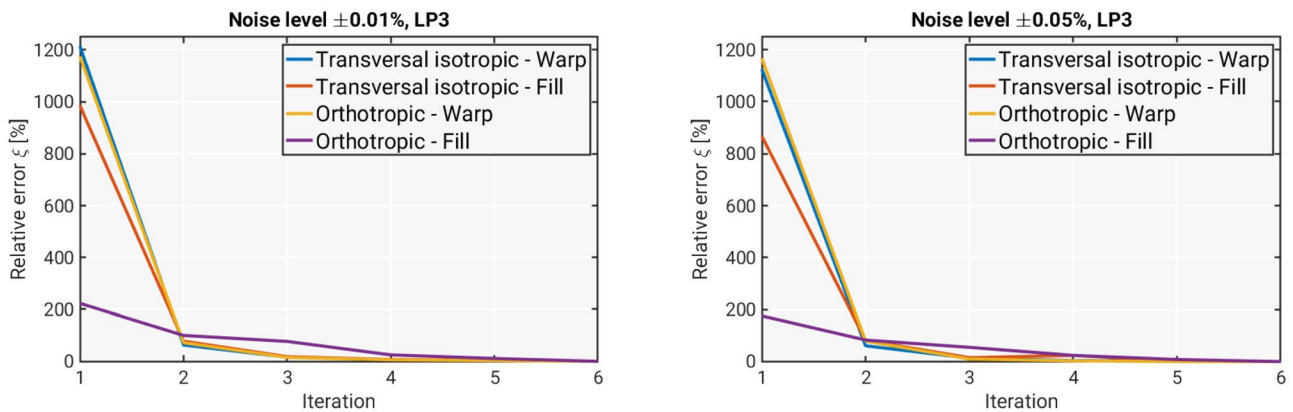
Coated woven fabric

The analysis is carried out for loading protocol 3 (LP3), where the distributions of the vertical, the radial and the tangential components of reaction forces on the circular disk obtained by solving the forward problem are shown in Fig. 12. A uniform distribution of the vertical and tangential forces as well as zero radial forces are considered as initial condition. Figure 13 shows the relative error measure ξ versus iteration number. As can be seen, the iterative scheme converges quite fast again. Regardless of the noise range being ±0.01% or ±0.05%, five iterations are needed to correct the reaction forces' distribution and

Fig. 11 Relative error measure ξ plotted along the iteration number considering the iterative EGM scheme for loading protocol 2 (LP2) applied to a calendered rubber specimen. As can be seen, very few iterations are needed to correct the distribution of the reaction forces on the cylindrical punch
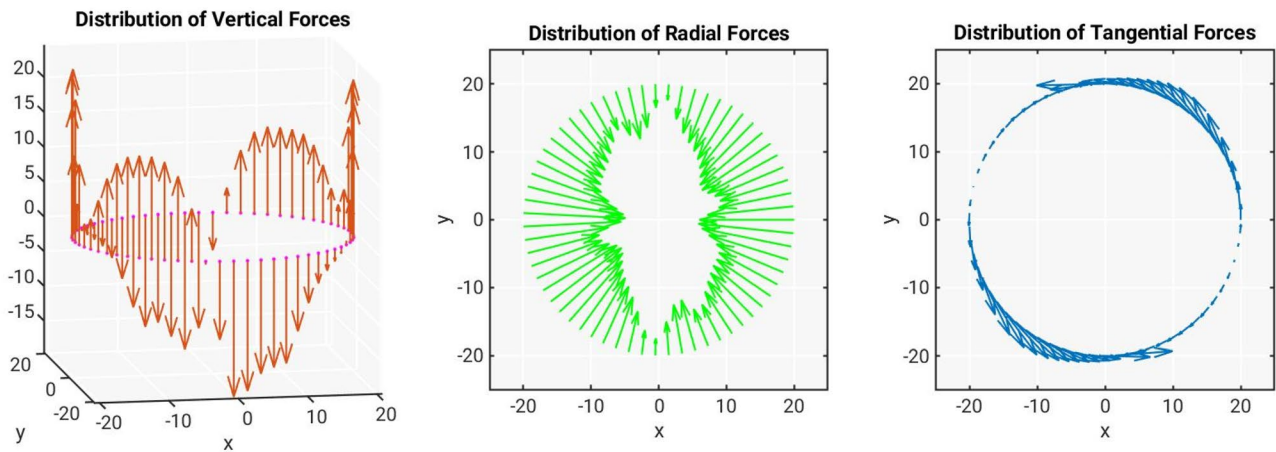
Fig. 12 Distribution of the reaction forces on the cylindrical punch resulting from the simulation using the prescribed parameters considering loading protocol 3 (LP3) and a specimen made from coated fabric

Fig. 13 Relative error measure ξ plotted versus iterations needed to correct the distribution of the reaction forces on the cylindrical punch considering the iterative EGM scheme for LP3 applied on a coated woven fabric specimen

determine the corresponding set of parameters. The relative error regarding the parameter values is presented in Table 3. For noise range 0.01%, the difference between these values and the relative error between the parameters obtained using the exact distribution of the forces and the prescribed parameters is negligible. While for a higher noise range, the parameters are obtained with relative error being a few percents higher than the relative error for the parameters obtained using the prescribed exact distribution of the reaction forces. Compared to the case of calendered rubber, the iterative EGM scheme requires slightly more iterations for the correction of the reaction forces which is most probably due to the more pronounced anisotropy of the textile membrane leading to a more heterogeneous distribution of the forces.

Discussion and Conclusion

This work presented an experimental-numerical framework to uniquely identify stiffness parameters for anisotropic nonlinear materials based on full-field measurements on a single experiment. Two direction-dependent materials have been analyzed to verify the proposed approach, starting from a two-parameter material model of calendered rubber to a more complex, four-parameter material model of woven textile fabric. A nonlinear anisotropic strain energy density function has been chosen from the literature to describe the mechanical behavior of the materials of interest. This model has been reformulated to be linear in the material parameters. Thereby, based on the Equilibrium Gap Method, a quadratic objective function for the identification of the (linear) stiffness-related material parameters could

be formulated enabling a unique identification procedure. Since measured full-field data on the displacements are included, this objective function corresponded to distances from mechanical equilibrium which are only governed by the choice of parameter values. Thus, by minimizing the objective function, the specific parameter values were computed which fulfill mechanical equilibrium as close as possible and thus, allow for those parameters which most accurately describe reality. In order to make sure that sufficient variation in deformations are included in one single experiment to address the nonlinearity in the material model, a novel experimental setup has been designed. Since the distributions of boundary forces, which are at least in parts essential for the EGM, can hardly be measured, a new iterative scheme has been proposed to stepwise correct an initially assumed uniform distribution. The feasibility of the proposed approach to indeed allow for a suitable parameter identification has been investigated for two anisotropic material classes: calendered rubber and coated woven textile fabric. To this end, virtual experiments were considered where material parameter values were predefined and used in a numerical simulation of the experiment. The resulting displacement field was then used as virtual experimental data and the prescribed parameters were considered as reference values to be obtained from the proposed approach. That way, a quantitative estimation of the performance of the method itself has been enabled. Real experimental data would not allow for such analysis because the optimal parameter values are not known. Have in mind that classical experiments and identification procedures are not necessarily more accurate as the method proposed here. In fact, the heterogeneous full-field kinematics included in our approach provide much more information about the material response than a selected number of biaxial tests with predefined stress- or strain ratios. Different cases of loading conditions and levels of noise included in the virtually measured displacement field were considered in our investigation leading to the following conclusions:

- *Influence of noisy full-field displacements:* For the calendered rubber, the parameters were identified with a maximum relative error of 33% when employing loading protocol 1 (application of vertical displacements only) and a noise range of 0.01%. For loading protocol 2 (vertical displacements combined with torsion) significantly improved results were obtained: a maximum error of 0.4% for noise range 0.01% and 4% for noise range 0.05%. For the coated woven fabric, applying loading protocol 1 was not sufficient at all to specifically identify the parameter associated with the fill direction since the corresponding nonlinearity turned out not to be sufficiently activated in the experiment. Loading protocol 2, instead, returned acceptable results with a maximum relative error of 8% for noise range 0.01%. However, the maximum relative error remains high with 97% for noise range 0.05%. By taking into account loading protocol 3, where a modified outer clamping of the

sheet allowed more deformation of the sheet, and by suitably selecting the considered deformation states, significant improvements could be achieved. Then the maximum relative errors 2% and 31% for noise ranges 0.01% and 0.05%, respectively, were found. Results showed that an accurate parameter identification could be achieved based on the proposed single experiment even for highly anisotropic and nonlinear thin sheets. For the experimental setup, it turned out to be important to allow for as large deformations of the specimen as possible. Therefore, some a priori knowledge regarding the qualitative material response is favorable. Our analysis showed that if a much stiffer direction is already known for a specific material class, then the specimen should not be externally clamped in this direction. If a material is already known to stiffen with larger deformations, it is beneficial to concentrate the deformation states considered in the EGM to the stiffening regime of deformations. This a priori knowledge should, however, not be considered a strong limitation of the proposed approach since a priori information regarding the qualitative response is practically always available. For instance, for the coated fabric, it is generally known that the warp direction is much stiffer than the fill direction. If for some very new material class no a priori knowledge is available, then the quality of the identified parameters can be quantitatively assessed by comparing the displacements obtained from a computational simulation (forward problem) using the identified parameters with the displacements from the experiment. If there is a large gap, this either means that the considered material model is not appropriate or that the experimental setup is not sufficiently adapted to the response of the specific material class. In the latter case, some classical biaxial tests could be considered to obtain the a priori knowledge. However, this does not represent a limitation of the proposed method since only very general qualitative a priori knowledge would become important in that case. Detailed quantitative parameter identification for a variety of different materials from this specific material class could then be more efficiently obtained from the proposed approach.

- *Unknown distribution of reaction forces at the boundary of the circular punch:* The performance of the iterative EGM scheme has been analyzed for the two material classes. A simple assumption of uniform/zero force distributions as initial guess for the iterative scheme turned out to be sufficient to accurately correct the real distributions and obtain suitable parameter values after quite few iterations. Using loading protocol 2 on the calendered rubber resulted in a low maximum relative error of 0.4% for the realistic noise range 0.01. For the coated fabric, also a low maximum error of 2% could be achieved for noise range 0.01 when applying loading protocol 3.

- *General performance:* Our analyses have shown that the proposed method turned out to be feasible for the accurate

identification of stiffness-related parameters of anisotropic, nonlinear thin sheets. One major advantage of the proposed approach is the unique identification allowing for a quantitative assessment and interpretation of the parameter values. Another major advantage is that only one single experiment is required for parameter identification which is in contrast to classical approaches based on e.g., biaxial tests. This was enabled by including full-field measurements on a specimen which is strongly inhomogeneously deformed. While this allowed for the before-mentioned advantages, providing accurate full-field measurements becomes essential. In parts of our analysis, Gaussian noise on the displacement field with maximum deviations of 0.05% did not allow for sufficiently accurate parameter identification. Even if nowadays measurements with less noise are possible, the influence of noise in the measured full-field data could easily be reduced by smoothening the measured displacement data before computing its spatial gradients needed for the evaluation of the material model. We did not include any smoothening in our analysis, in order to capture the worst case scenario to indeed challenge our approach. As a final advantage of the proposed method, its efficiency should be pointed out. Although full-field data is included, the iterative EGM allows a suitable parameter identification by just computing a very small number of 3-5 forward problems, i.e. computational simulation of the experiment, since these are only required in each iteration step.

Appendix 1 Continuum Mechanical Basis and FE Discretization

This mechanical problem is formulated in the context of continuum mechanics at finite strains [44], where Ω_0 and Ω are considered to be the body of interest in the (undeformed) reference and the (deformed) current configurations, respectively, parameterized by the position vectors X and x. The displacement of the material points can then be defined as $u = x - X$. As measure for the deformations, we consider the right Cauchy-Green deformation tensor

$$C = F^T F \quad \text{with} \quad F := 1 + \text{Grad}[u] \quad \text{and} \quad J := \det F > 0 \tag{18}$$

being the deformation gradient and the Jacobi determinant, respectively. 1 denotes the second-order identity tensor. In the context of hyperelasticity, the stresses are computed as derivative of a strain energy density function $\psi := \psi(C)$ with respect to the deformation tensor. In detail, the second Piola-Kirchhoff stress tensor S, and based thereon, the Cauchy stress tensor σ, known as physical stresses, and the 1st Piola-Kirchhoff tensor P, known as technical stresses, are computed by

$$S = 2\frac{\partial \psi}{\partial C}, \quad \sigma = J^{-1} F S F^T, \quad \text{and} \quad P = FS, \tag{19}$$

respectively. We are interested in the analysis of boundary value problems to identify material parameters included in the mechanical model based on full-field kinematics. To define these boundary value problems we consider the principle of the minimum of the total potential energy Π which has to be minimized with respect to the displacement vectors u, i.e.,

$$\Pi(u) = \int_{\Omega_0} \psi(C(\nabla u)) dV - \int_{\partial \Omega_0} u \cdot t \, dA \quad \rightarrow \quad \min_u, \tag{20}$$

wherein t denotes the traction vector at the surface. Note that inertia and volume forces are neglected here since their contribution can be considered negligible for slow deformation processes and thin materials. The necessary condition for minimum total potential energy is that the first variation vanishes. Inserting the first variation of the strain energy density $\delta\psi = \frac{1}{2} 2\partial_C \psi \cdot \delta C = \frac{1}{2}\delta C \cdot S$, we obtain

$$\delta\Pi(u) = \int_{\Omega_0} \frac{1}{2}\delta C \cdot S \, dV - \int_{\partial\Omega_0} \delta u \cdot t \, dA = 0, \tag{21}$$

where δu denotes the variation of u. The solution of (21) is here obtained using the FE method considering hexahedral elements with tri-linear shape functions. Having in mind that the considered sheets are rather thin, also shell elements may be considered instead, see e.g., [45]. We consider the classical matrix of shape functions N_e and the B-matrix B_e containing the derivatives of the shape functions with respect to the coordinates for the approximation of the right Cauchy-Green tensor and the displacements in terms of nodal displacements d_e and nodal variations δd_e per element e, respectively. Then, we decompose the whole body Ω_0 into finite elements Ω_0^e and insert $\frac{1}{2}\delta C \approx B_e \delta d_e$ and $\delta u \approx N_e d_e$ into (21) to obtain

$$\delta\Pi = \sum_e \delta d_e^T \left(r_e^{\text{int}} - r_e^{\text{ext}} \right) = 0 \quad \text{with}$$

$$r_e^{\text{int}} := \int_{\Omega_0^e} B_e^T S \, dV \quad \text{and} \quad r_e^{\text{ext}} := \int_{\partial\Omega_0^e} N_e^T t \, dA, \tag{22}$$

with r_e^{int} and r_e^{ext} denoting the internal and external nodal forces per element. Note that Voigt matrix notation is used here and everywhere in the sequel whenever FE-discretized equations are considered. Following standard procedure to unify all nodal displacement variations into a global vector of nodal variations δD and to assemble all nodal force vectors on element level to the global counterparts R^{int} and R^{ext}, we obtain

$$\delta D^T R = 0 \quad \text{with} \quad R := R^{\text{int}} - R^{\text{ext}}. \tag{23}$$
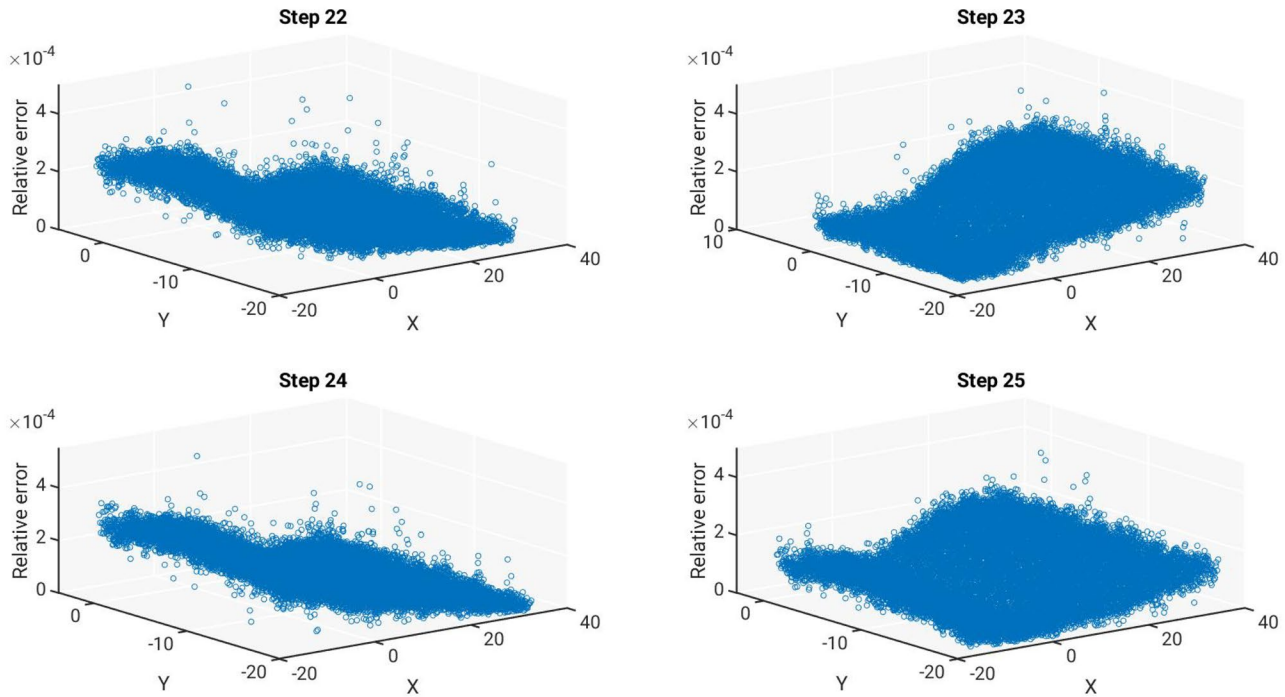
Fig. 14 Relative error of the displacement field obtained from Digital Image Correlation on a specimen moved successively 25 mm in horizontal direction. The relative error is plotted at the last four steps of the total displacements. The X and Y axis are the positions of the plate in space, and the Z axis is the relative error for each measurement point

Incorporating given Dirichlet boundary conditions in $\delta\mathbf{D}$ and noticing that the variations can take arbitrary values at all nodes except the ones at the Dirichlet boundary, mechanical equilibrium of forces is fulfilled if the internal forces match the external forces, i.e. $\mathbf{R} = \mathbf{R}^{\text{int}} - \mathbf{R}^{\text{ext}} = \mathbf{0}$.

Appendix 2 Assessment of Accuracy of DIC Measurements

The displacement field obtained from DIC measurements is subjected to a relative error, which has been found to be ranging from $0.01\% - 0.05\%$, cf. [43]. In order to verify this and justify the applied noise levels in our analysis, a performance test has been conducted at the Continuum Mechanics laboratory at Ruhr University Bochum to assess the accuracy of the DIC system in detecting displacement fields. In this test, a plate sprayed with a speckle pattern is placed on a sliding stage and successively moved 25 mm horizontally. Two CCD cameras are synchronized and built to capture the upper surface of the specimen during the deformation with image acquisition occurring every 1 mm, resulting in a total of 25 images. Then, the relative error of the measured and known (applied) displacement is computed for each point in space, i.e. each point in the images. The resulting spatial distribution of the relative errors is plotted in Fig. 14 for the last four deformation steps. The results show that the relative error in the displacement

measurements provided by the system falls within the range of $0.01\% - 0.03\%$, with a few points reaching 0.04%. However, for a significant fraction of positions (almost the half of the plate), a relative error around 0.01% or below is obtained.

Appendix 3 Effect of the Number of States Included in the Objective Function

The effect of the number of recorded loading states M included in the objective function on the identified parameters is analyzed. Considering loading protocol 1 (LP1) with 16 mm applied vertical displacements applied on the calendered rubber specimen and a noise range of $\pm 0.01\%$, we examine 50, 20 and 10 states along the deformation process. The relative error for each parameter is reported in Table 4 corresponding to each M. It can be noted, that larger

Table 4 Relative error of the identified parameters for the calendered rubber for loading protocol 1, where noise range $\pm 0.01\%$ and various numbers of load steps M is analyzed. LP1 refers to the case where purely vertical displacements are considered. The impact of the resulting parameters on the material behavior is shown in Fig. 15

Scenario	$\eta(\alpha_{\text{c}})$	$\eta(\alpha_{\text{t}})$
LP1, $M = 50$, noise range $\pm 0.01\%$	0.38	0.21
LP1, $M = 20$, noise range $\pm 0.01\%$	0.35	0.20
LP1, $M = 10$, noise range $\pm 0.01\%$	0.33	0.18
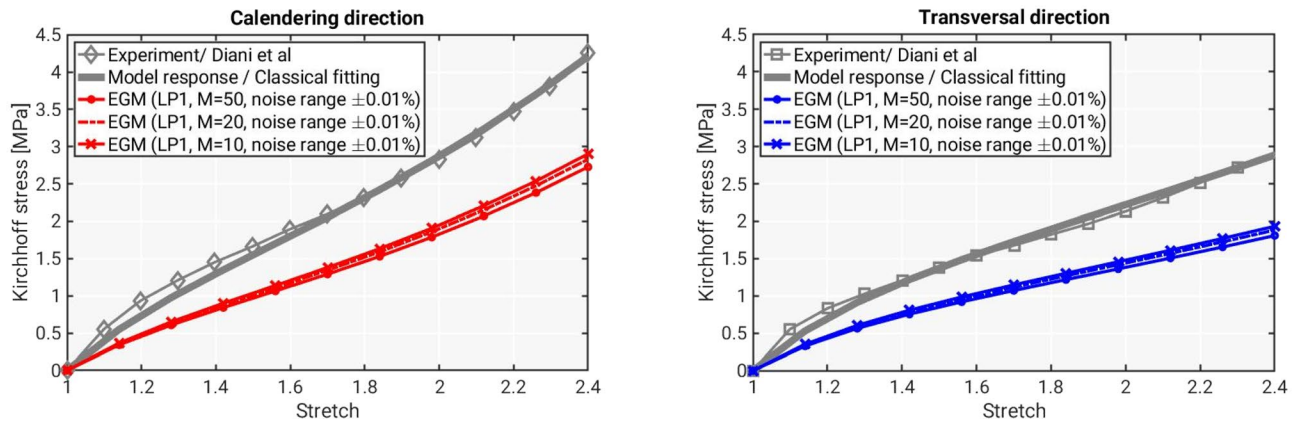
Fig. 15 Calendered rubber specimen under uniaxial tension: comparison of experimental data and model response evaluated for sets of parameters obtained by including different numbers of load steps M for load protocol LP1, where solely vertical displacements are applied in the experimental setup. As can be seen, a poor representation of the classical experiment is obtained when identifying the parameters based on LP1

numbers of the considered deformation states lead to larger errors in the values of the identified parameters, varying from maximum 38% to 33% for $M = 50$ to $M = 10$, respectively. In fact, one would expect that the larger the number of considered deformation states is, the larger is the content of deformation information and thus, the better the parameter identification. However, at the same time, the amount of noise added to the identification procedure is increased. As a consequence, one has to make a trade-off when choosing the number of states to be used in the identification. The model response evaluated for the parameters resulting from the EGM for different numbers of considered states is plotted together with the experimental data in Fig. 15. Following the results obtained here, the identification results presented in the remainder of the paper are obtained by considering $M = 10$ states along the deformation process.

Declarations

Conflict of Interest The authors declare that they have no conflicts of interest and did not involve human or animal participants in their study.

References

1. Ogden R, Saccomandi G, Sgura I (2004) Fitting hyperelastic models to experimental data. Comput Mech 34:484–502. https://doi.org/10.1007/s00466-004-0593-y
2. Treloar LRG (1944) Stress-strain data for vulcanized rubber under various types of deformation. Rubber Chem Technol 4(17):813–825
3. Johlitz M, Diebels S (2011) Characterisation of a polymer using biaxial tension tests. part i: Hyperelasticity. Arch Appl Mech 81:1333–1349. https://doi.org/10.1007/s00419-010-0480-1
4. Diani J, Brieu M, Vacherand J, Rezgui A (2004) Directional model for isotropic and anisotropic hyperelastic rubber-like materials. Mech Mater 36:313–321
5. Labus K, Puttlitz C (2016) An anisotropic hyperelastic constitutive model of brain white matter in biaxial tension and structural-mechanical relationships. J Mech Behav Biomed Mater 62:195–208
6. Peng X, Guo G, Zhao N (2013) An anisotropic hyperelastic constitutive model with shear interaction for cord-rubber composites. Compos Sci Technol 78:69–74. https://doi.org/10.1016/j.compscitech.2013.02.005
7. Balzani D, Neff P, Schröder J, Holzapfel GA (2006) A polyconvex framework for soft biological tissues. Adjustment to experimental data. Int J Solids Struct 43:6052–6070
8. Guerin H, Elliott D (2006) Quantifying the contributions of structure to annulus fibrosus mechanical function using a nonlinear, anisotropic, hyperelastic model. J Orthop Res 25(25):508–516. https://doi.org/10.1002/jor.20324
9. Motevalli M, Uhlemann J, Stranghöner N, Balzani D (2019) Geometrically nonlinear simulation of textile membrane structures based on orthotropic hyperelastic energy functions. Compos Struct 223:110908
10. Uhlemann J, Surholt F, Westerhoff A, Stranghöner N, Motevalli M, Balzani D (2020) Saturation of the stress-strain behavior of architectured fabrics. Mater Des 191:108584. https://doi.org/10.1016/j.matdes.2020.108584

11. Motevalli M, Uhlemann J, Stranghöner, Balzani D (2020) The elastic share of inelastic stress-strain paths of woven fabrics. Materials 13:4243. https://doi.org/10.3390/ma13194243

12. Avril S, Bonnet M, Bretelle A, Grediac M, Hild F, Ienny P, Latourte F, Lemosse D, Pagano S, Pagnacco E, Pierron F (2008) Overview of identification methods of mechanical parameters based on full-field measurements. Exp Mech 48:381–402

13. Kavanagh KT, Clough RW (1971) Finite element applications in the characterization of elastic solids. Int J Solids Struct 7:11–23

14. Pagnacco E, Moreau A, Lemosse D (2007) Inverse strategies for the identification of elastic and viscoelastic material parameters using full-field measurements. Mater Sci Eng 452–453:737–745

15. Schmaltz S, Willner K (2014) Comparison of different biaxial tests for the inverse identification of sheet steel material parameters. Strain 50:389–403

16. Giton M, Caro-bretelle AS, Ienny P (2006) Hyperelastic behaviour identification by a forward problem resolution: application to a tear test of a silicone-rubber. Strain 42:291–297

17. Pagnacco E, Lemosse D, Hild F, Amiot F (2006) Inverse strategy from displacement field measurement and distributed forces using FEA. SEM Annual Conference And Exposition On Experimental And Applied Mechanics, Portland 24:13

18. Ladeveze P, Leguillon D (1983) Error estimate procedure in the finite element method and applications. SIAM J Numer Anal 20:485

19. Grédiac M, Pierron F, Avril S, Toussaint E (2006) The virtual fields method extracting constitutive parameters from full-field measurements: a review. Strain 42:233–253

20. Mei Y, Liu J, Zimmermann B, Nguyen T, Avril S (2021) General finite-element framework of the virtual fields method in nonlinear elasticity. J Elast 145:265–294

21. Deng J, Guo X, Mei Y, Avril S (2023) Fenics implemetation of the virtual fields method (VFM) for nonhomogeneous hyperelastic identification. Adv Eng Softw 175:103343

22. Ikehata M (1990) Inversion formulas for the linearized problem for an inverse boundary value problem in elastic prospection. SIAM J Appl Math 50:1635–1644

23. Grédiac M, Hild F (2012) Full-field measurements and identification in solid mechanics. John Wiley & Sons

24. Crouzeix L, Perie JN, Collombet F, Douchin B (2009) An orthotropic variant of the equilibrium gap method applied to the analysis of a biaxial test on a composite material. Compos A 40:1732–1740

25. Colasante G (2014) Tensile structures: biaxial testing and constitutive modelling of coated fabrics at finite strains. Ph.D. Thesis, Politechnico di Milano

26. Holzapfel GA, Gasser T, Ogden R (2000) A new constitutive framework for arterial wall mechanics and a comparative study of material models. 61:1–48

27. Itskov M, Aksel N (2004) A class of orthotropic and transversely isotropic hyperelastic constitutive models based on a polyconvex strain energy function. Int J Solids Struct 41:3833–3848

28. Schröder J, Neff P (2003) Invariant formulation of hyberelastic transvere isotropiy based on polyconvex free energy functions. Int J Solids Struct 40:401–445

29. Schröder J, Neff P, Ebbing V (2008) Anisotropic polyconvex energies on the basis of crystallographic motivated structural tensors. J Mech Phys Solids 56:3486–3506

30. Perotti L, Ponnaluri A, Krishnamoorthi S, Balzani D, Ennis D, Klug W (2017) Method for the unique identification of hyperelastic material properties using full-field measures. Application to the passive myocardium material response. Numer Method Biomed Eng 33:e2866

31. Motevalli M, Balzani D (2023) Efficient identification of material parameters for an orthotropic hyperelastic nonlinear material model for textile membranes. Constr Build Mater 378:131114. https://doi.org/10.1016/j.conbuildmat.2023.131114

32. Uhlemann J, Stranghöner N, Motevalli M, Balzani D (2021) Architectural woven polyester fabrics: examination of possible classification of stiffness values in correlation with strength values. Archit Eng Des Manag 17(3–4):281–298. https://doi.org/10.1080/17452007.2020.1793720

33. Schröder J, Neff P, Balzani D (2005) A variational approach for materially stable anisotropic hyperelasticity. Int J Solids Struct 42(15):4352–4371. https://doi.org/10.1016/j.ijsolstr.2004.11.021

34. Chu TC, Ranson WF, Sutton MA, Peters WH (1985) Application of digital-image-correlation techniques to experimental mechanics. SIAM J Appl Math 25:232–244

35. Sutton M, Orteu J, Schreier H (2009) Image correlation for shape, motion and deformation measurements: basic concepts, theory and applications. Springer

36. Sutton M, Yan J, Tiwari V, Schreier H, Orteu J (2008) The effect of out-of-plane motion on 2D and 3D digital image correlation measurements. Opt Lasers Eng 46:746–757

37. Pan B, Qian K, Xie H, Asundi A (2009) Two-dimensional digital image correlation for in-plane displacement and strain measurement: a review. Meas Sci Technol 20:17

38. Orteu J (2009) 3-D computer vision in experimental mechanics. Opt Lasers Eng 47:282–291

39. Motevalli M, Uhlemann J, Stranghöner N, Balzani D (2019) A new nonlinear polyconvex orthotropic material model for the robust simulation of technical fabrics in civil engineering applications at large strains - validation with large-scale experiment. Bauingenieur 94(2):488–497

40. Bridgens BN, Gosling PD (2010) Interpretation of results from the MSAJ testing method for elastic constants of membrane materials. Proceedings of the TensiNet Symposium pp 49–57

41. Galliot C, Luchsinger R (2009) A simple model describing the non-linear biaxial tensile behaviour of PVC-coated polyester fabrics for use in finite element analysis. Compos Struct 90:438–447. https://doi.org/10.1016/j.compstruct.2009.04.016

42. Uhlemann J (2016) Elastic constants of architectural fabrics for design purposes. Thesis for: PhD 4:438–447. https://doi.org/10.2370/9783844044492

43. Becker T, Splitthof K, Siebert T, Kletting P (2006) Error estimations of 3D digital image correlation measurements. SPIE 6341:86–91

44. Truesdell C, Noll W (1965) The non-linear field theories of mechanics. Springer

45. Balzani D, Gruttmann F, Schröder J (2008) Analysis of thin shells using anisotropic polyconvex energy densities. Comput Methods Appl Mech Eng 197:1015–1032